Science Signaling
AAAS

` A Dynamic Network Model of mTOR Signaling Reveals TSC-Independent mTORC2 Regulation

Piero Dalle Pezze, Annika G. Sonntag, Antje Thien, Mirja T. Prentzell, Markus Gödel, Sven Fischer, Elke Neumann-Haefelin, Tobias B. Huber, Ralf Baumeister, Daryl P. Shanley and Kathrin Thedieck (27 March 2012)
Science Signaling **5** (217), ra25. [DOI: 10.1126/scisignal.2002469]

COMPUTATIONAL BIOLOGY

A Dynamic Network Model of mTOR Signaling Reveals TSC-Independent mTORC2 Regulation

Piero Dalle Pezze,[1,2]* Annika G. Sonntag,[3]* Antje Thien,[4] Mirja T. Prentzell,[3] Markus Gödel,[4] Sven Fischer,[3] Elke Neumann-Haefelin,[4] Tobias B. Huber,[4,5] Ralf Baumeister,[3,5,6,7] Daryl P. Shanley,[1,2]† Kathrin Thedieck[3,5,6]†

The kinase mammalian target of rapamycin (mTOR) exists in two multiprotein complexes (mTORC1 and mTORC2) and is a central regulator of growth and metabolism. Insulin activation of mTORC1, mediated by phosphoinositide 3-kinase (PI3K), Akt, and the inhibitory tuberous sclerosis complex 1/2 (TSC1-TSC2), initiates a negative feedback loop that ultimately inhibits PI3K. We present a data-driven dynamic insulin-mTOR network model that integrates the entire core network and used this model to investigate the less well understood mechanisms by which insulin regulates mTORC2. By analyzing the effects of perturbations targeting several levels within the network in silico and experimentally, we found that, in contrast to current hypotheses, the TSC1-TSC2 complex was not a direct or indirect (acting through the negative feedback loop) regulator of mTORC2. Although mTORC2 activation required active PI3K, this was not affected by the negative feedback loop. Therefore, we propose an mTORC2 activation pathway through a PI3K variant that is insensitive to the negative feedback loop that regulates mTORC1. This putative pathway predicts that mTORC2 would be refractory to Akt, which inhibits TSC1-TSC2, and, indeed, we found that mTORC2 was insensitive to constitutive Akt activation in several cell types. Our results suggest that a previously unknown network structure connects mTORC2 to its upstream cues and clarifies which molecular connectors contribute to mTORC2 activation.

INTRODUCTION

The kinase target of rapamycin (TOR) is conserved in all eukaryotes from yeast to humans and is a central regulator of cellular growth, aging, and metabolism (*1*, *2*). As a central metabolic regulator, TOR is involved in a multitude of human diseases, including metabolic syndromes, cancer, and neurodegenerative diseases (*1*). Rapamycin is a well-known immunosuppressant, and rapalogs and other TOR inhibitors are applied in cancer therapy (*3*). Because of its clinical importance, it is important to understand the exact dynamics and interconnections within the TOR network.

TOR occurs in two functionally and structurally distinct multiprotein complexes termed TOR complex 1 (TORC1) and TORC2. The mammalian TORC1 (mTORC1) contains the specific scaffold protein Raptor and the inhibitory binding partner PRAS40, whereas mTORC2 contains the proteins Rictor, mSin1, PRR5, and PRR5L (*1*). mTORC1 controls cellular growth, translation, transcription, and autophagy (*4*); mTORC2 controls spatial growth by regulating the actin cytoskeleton (*5*). mTORC1 is specifically inhibited by the small macrolide rapamycin, whereas mTORC2 is rapamycin-insensitive. Adenosine triphosphate (ATP) analog TOR kinase inhibitors (TORKinibs) that target both mTOR complexes have also been described (*6*). Although the upstream and downstream regulatory mechanisms controlling mTORC1 are well characterized, those regulating mTORC2 are less well understood.

mTORC1 is regulated by nutrients (amino acids), growth factors (insulin), and energy (*7*). Amino acids activate the Ragulator-Rag complex to translocate mTORC1 to lysosomes, where mTORC1 can be activated by the small guanosine triphosphatase (GTPase) Rheb (*8*–*10*). Insulin signaling induces a kinase cascade through the insulin receptor (IR), IR substrate (IRS), class I phosphoinositide 3-kinases (PI3Ks), phosphoinositide-dependent protein kinase 1 (PDK1), and the AGC kinase Akt (also known as PKB). Akt inhibits the tuberous sclerosis complex 1/2 (TSC1-TSC2) dimer, which is the inhibitory GTPase-activating protein (GAP) for Rheb (*4*). Through this cascade, Akt stimulates mTORC1 activity. The best-characterized mTORC1 substrates are the AGC kinase p70 ribosomal protein S6 kinase (p70S6K), the translation initiation regulator 4E binding protein (4E-BP), and the proline-rich Akt substrate PRAS40, which is an inhibitor of mTORC1 (*11*). By binding mTORC1, PRAS40 contributes to the inhibition of mTORC1 activity (*12*–*16*). In response to insulin, Ser^{183} of PRAS40 is phosphorylated by mTORC1 (*17*), which releases PRAS40 from the complex and relieves its inhibitory effect on mTORC1 (*18*), allowing mTORC1 to phosphorylate its downstream substrates p70S6K and 4E-BP and promote cellular growth. Furthermore, there is a negative feedback loop (NFL) that inhibits upstream insulin signaling upon mTORC1 activation: Active p70S6K phosphorylates and inhibits IRS, which prevents activation of PI3K in response to insulin (*4*).

mTORC2 is mainly regulated by growth factors (*1*), although induction by nutrients has also been described (*19*, *20*). Little is known about the molecular mechanism by which insulin induces mTORC2. The known substrates of mTORC2 are the AGC kinases Akt (*21*–*24*), serum- and glucocorticoid-induced protein kinase SGK (*25*), and protein kinase C α (PKCα) (*26*). AGC kinases must be phosphorylated twice to be fully active (*27*–*29*): They are phosphorylated by PDK1 in the T loop and in

[1]Institute for Ageing and Health, Newcastle University, Campus for Ageing and Vitality, Newcastle upon Tyne NE4 5PL, UK. [2]Centre for Integrated Systems Biology of Ageing and Nutrition, Institute for Ageing and Health, Newcastle University, Newcastle upon Tyne NE4 5PL, UK. [3]Bioinformatics and Molecular Genetics (Faculty of Biology), Albert-Ludwigs-Universität Freiburg, 79104 Freiburg, Germany. [4]Renal Division, University Hospital Freiburg, 79106 Freiburg, Germany. [5]BIOSS Centre for Biological Signalling Studies, Albert-Ludwigs-Universität Freiburg, 79104 Freiburg, Germany. [6]Center for Systems Biology (ZBSA), Albert-Ludwigs-Universität Freiburg, 79104 Freiburg, Germany. [7]ZBMZ (Faculty of Medicine) and Freiburg Institute for Advanced Studies (FRIAS), Albert-Ludwigs-Universität Freiburg, 79104 Freiburg, Germany.
*These authors contributed equally to this work.
†To whom correspondence should be addressed. E-mail: kathrin.thedieck@biologie.uni-freiburg.de (K.T.); daryl.shanley@newcastle.ac.uk (D.P.S.)

the hydrophobic motif by a PDK2. Only one PDK1 exists for all AGC kinases, but the identity of PDK2 differs among the AGC kinases. mTORC2 is a PDK2 for Akt, SGK, and PKCα (*27*–*29*), and phosphorylation of Ser^{473} of Akt is a commonly used readout for mTORC2 activity.

Using mTORC2 substrate AGC kinases as indicators of mTORC2 activity, the TSC1-TSC2 complex has been implicated in mTORC2 activation by insulin: TSC1-TSC2 inhibition reduces phosphorylation of the mTORC2 substrate Akt at Ser^{473} (*30*–*33*). This result was surprising because TSC1-TSC2 inhibits mTORC1 (*34*). Two models have been proposed to explain mTORC2 regulation by TSC1-TSC2, involving either direct mTORC2 activation by TSC1-TSC2 (*31*, *33*) or an indirect mechanism through an active NFL that inhibits PI3K when mTORC1 was hyperactive in response to TSC1-TSC2 ablation (*35*). However, data showing that mTORC2 contributes to proliferation in TSC2-null cells suggest that mTORC2 can be active in the absence of TSC1-TSC2 (*36*). A third hypothesis for mTORC2 activation is through a PI3K-independent mechanism, which has been identified in *Dictyostelium* (*37*–*40*). In mammals, several cellular processes that are regulated by mTORC2 have been described as PI3K-independent (*19*, *26*, *41*–*43*), making the hypothesis of PI3K-independent activation of mTORC2 conceivable.

To distinguish among the possible mTORC2 activation mechanisms and to determine whether they acted independently or in combination, we developed a mathematical dynamic network model. We hypothesized that different modes of mTORC2 regulation would result in distinguishable, dynamic network responses. With the mathematical model, we performed specific predictive dynamic simulations for alternative mechanisms of mTORC2 regulation, and then these were experimentally validated.

There are several computational studies related to mTOR signaling. These include static network models of known molecular interactions, for example, the map for the insulin-mTOR network (*44*). Dynamic models also exist. These require information about the molecular interactions and also detailed quantitative experimental time course data, which can be generated specifically for the model (*45*–*53*) or can use data from previous studies (*45*, *54*–*57*). Much of the currently available dynamic models focus on the upstream insulin signaling events, such as the binding of insulin to its receptor (*50*), and receptor autophosphorylation and receptor-mediated substrate phosphorylation, together with receptor cycling and endocytosis (*46*, *49*). More extensive models including activation of IRS, PI3K, Akt, and the NFL have been developed with specific functional emphasis on cycling of the glucose transporter GLUT4 (*54*), dendritic protein synthesis (*45*), or breast cancer therapy (*51*). Other models address complex issues, such as joint regulation of the NFL by insulin and amino acids (*56*), crosstalk with epidermal growth factor (EGF) signaling and the mitogen-activated protein kinase (MAPK) pathway (*48*), and TORC1 regulation by phosphatases in yeast (*52*). Because the combined experimental-computational approaches typically address specific questions, the generated data sets are often limited, representing one (*47*) or two time points (*53*), or representing limited parts of the network, such as binding of insulin and insulin-like growth factor (IGF) to their receptors (*50*). None of the existing models integrates mTORC2 regulation.

Here, we report an insulin-mTOR network model integrating both mTORC1 and mTORC2. The model was parameterized with dynamic quantitative time course data and experimentally validated. Subsequently, we introduced in silico and experimental network perturbations to simulate and experimentally test alternative network structures connecting mTORC2 to upstream insulin signaling. This approach provides the benefit of both a structural and a dynamic network analysis (*58*).

Our model and experimental testing indicated that in contrast to previous hypotheses, the TSC1-TSC2 complex was not a direct activator of mTORC2 and that mTORC2 activity was insensitive to the mTORC1-induced NFL. Furthermore, although PI3K is inhibited by the NFL, activation of the NFL-insensitive mTORC2 also required active PI3K. Hence, all three literature-based hypotheses were excluded by our combined simulation and experimental data. Instead, we postulate that insulin signaling activates mTORC2 through a PI3K that is insensitive to the NFL; thus, insulin triggers signaling networks that diverge upstream of Akt. We created a network structure that fits the available experimental data and provided experimental evidence supporting the network.

RESULTS

A dynamic insulin-regulated TOR network model

Initially, we established a static network model in SBGN (Systems Biology Graphical Notation) format (*59*) of insulin-mTOR signaling as a means to integrate current knowledge and as a platform to guide our decision on appropriate targets for measurement (fig. S1). The choice of boundaries for such a network and the level of molecular detail to include are subjective decisions. There is considerable existing knowledge concerning insulin signaling and the regulation of TOR (*1*, *7*). Although we used this information, we needed to minimize the amount of detail because precise dynamics for the extended graphical model could not be defined due to the high number of parameters and the difficulty in obtaining sufficient experimental data. Therefore, we abstracted the extended model on the basis of two main considerations. First, we selected regulation mechanisms with an important role in dynamic behavior, such as the activation of mTOR complexes by the presence of both amino acids and insulin, the pathways connecting these stimuli to the mTOR complexes, and the NFL from p70S6K to IRS. Second, we selected molecules and interactions that we could reliably measure. To capture the network dynamics upon starvation and in response to amino acids plus insulin (aa/insulin), we distributed our measurements widely across the network. We monitored the abundance of Tyr^{1146}-phosphorylated IR, Ser^{636}-phosphorylated IRS1, Ser^{473}- and Thr^{308}-phosphorylated Akt, Ser^{2448}- and Ser^{2481}-phosphorylated mTOR, Thr^{246}- and Ser^{183}-phosphorylated PRAS40, and Thr^{389}-phosphorylated p70S6K (see the selected targets marked with an asterisk in fig. S1).

On the basis of the molecules we could measure, we condensed our network structure to minimize poorly defined intermediate steps between obtainable data (Fig. 1A). The condensed network depicts insulin signaling propagating from the IR through the TSC1-TSC2 complex to the mTORC1 complex and includes p70S6K, PRAS40, and Akt. In addition, mTORC1 induction by amino acids was included. At this point, no upstream pathway regulating mTORC2 was assumed. This model formed the starting point for our dynamic study.

Readout selection for mTORC2 activity: Akt-pS^{473} and mTOR-pS^{2481}

Studies suggesting that TSC1-TSC2 regulates mTORC2 commonly used Akt phosphorylated at Ser^{473} (Akt-pS^{473}) as the mTORC2 readout. However, the phosphorylation of Akt depends on PI3K and the phosphatidylinositol 3,4,5-trisphosphate [PtdIns(3,4,5)P_3] generated by PI3K, which binds to Akt and triggers its relocalization to the plasma membrane, where Thr^{308} is phosphorylated by PDK1 and Ser^{473} is phosphorylated by mTORC2 (*27*). Thus, phosphorylation of Akt at either Thr^{308} or Ser^{473} depends on PI3K activity. PI3K and Akt are inhibited in the absence of the inhibitory TSC1-TSC2 complex because of hyperactivation of mTORC1

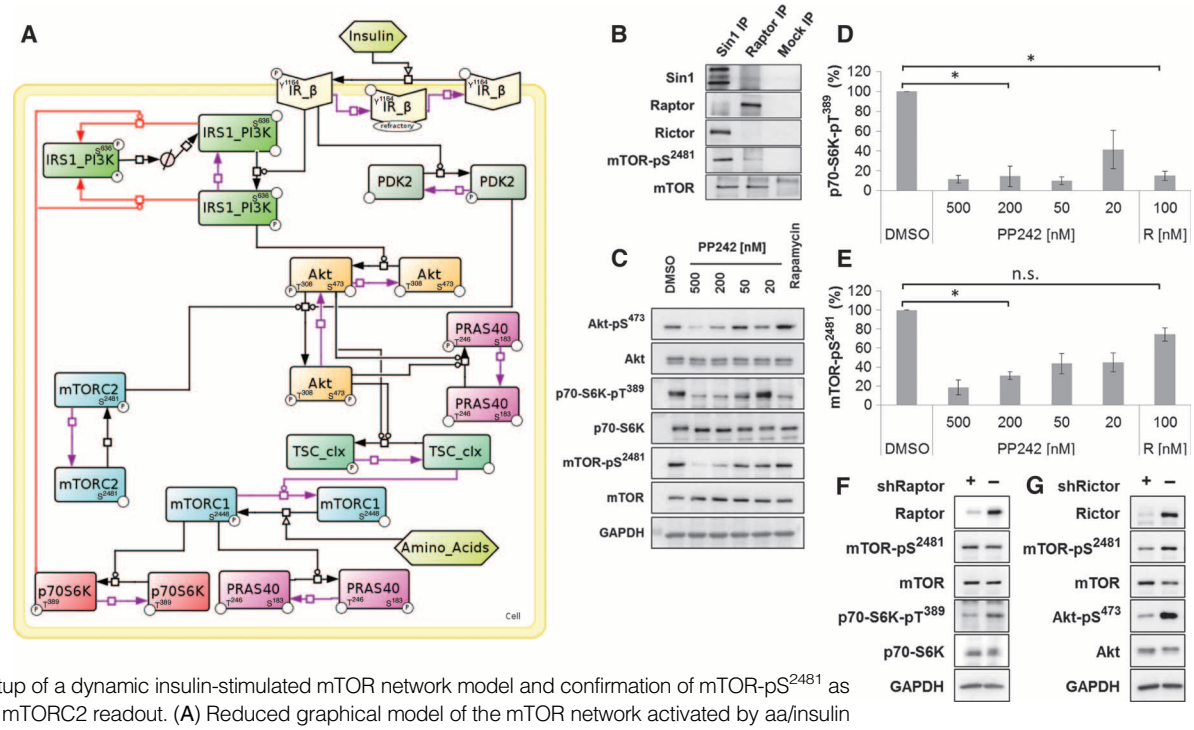

Fig. 1. Setup of a dynamic insulin-stimulated mTOR network model and confirmation of mTOR-pS^{2481} as a specific mTORC2 readout. (**A**) Reduced graphical model of the mTOR network activated by aa/insulin (see fig. S1 for the extended graphical model). (**B**) Coimmunoprecipitation (IP) of mTOR-pS^{2481} with Sin1 (a component of mTORC2) or Raptor (a component of mTORC1); Mock IP, control IP with a nonspecific antibody. Data are representative of three experiments. (**C**) Effect of PP242 or rapamycin on the indicated phosphorylated proteins. Data are representative of three experiments. (**D** and **E**) Quantitation of three experiments similar to the one shown in (C) for mTORC1 readout p70-S6K-pT^{389} (D) and mTORC2 readout mTOR-pS^{2481} (E). R, rapamycin. *$P < 0.05$; n.s., not significant. In (D), PP242 [200 nM, an mTOR-specific standard concentration (*6*)]–treated compared to dimethyl sulfoxide (DMSO)–treated control and rapamycin-treated samples compared to DMSO control were significant. In (E), PP242 (200 nM)–treated compared to DMSO-treated control was significant. Rapamycin (100 nM) compared to DMSO control was not significant. (**F**) Effect of Raptor knockdown on mTOR-pS^{2481}. Data are representative of three experiments. (**G**) Effect of Rictor knockdown on mTOR-pS^{2481}. Data are representative of three experiments.

and the NFL. Consequently, under conditions of TSC1-TSC2 deficiency and NFL activation, monitoring Akt-pS^{473} does not differentiate between PI3K, PDK1, and mTORC2 activity and therefore may not be a suitable readout to investigate the mode of mTORC2 regulation by TSC1-TSC2 (*32*). Other AGC kinases that are targeted by mTORC2 (SGK and PKCα) are not ideal because they have similar issues (*28*, *60*). The rapamycin-insensitive autophosphorylation of Ser^{2481} (mTOR-pS^{2481}) (*61*, *62*) has been described as mTORC2-specific (*63*) and as occuring in both the mTOR complexes (*64*). To determine whether mTOR-pS^{2481} is a better readout for mTORC2 activity than is the phosphorylation of AGC kinases and whether monitoring mTOR-pS^{2481} will distinguish between PI3K and mTORC2 activity, we determined that mTOR-pS^{2481} was a specific readout for mTORC2 activity in HeLa cells. We performed complex-specific immunoprecipitations with antibodies against Sin1 (for mTORC2) or Raptor (for mTORC1) and assessed the amount of mTOR-pS^{2481} that co-immunoprecipitated (Fig. 1B). In HeLa cells, mTOR-pS^{2481} was predominantly associated with mTORC2 and only weakly associated with mTORC1, suggesting that mTOR-pS^{2481} is a suitable readout of mTORC2 activity. Furthermore, whereas the mTORC1-specific readout p70S6K1-pT^{389} was reduced by the mTORC1-specific inhibitor rapamycin (Fig. 1, C and D), in agreement with Copp *et al.* (*63*), mTOR-pS^{2481} was not significantly affected by short-term treatment with the rapamycin (Fig. 1, C and E). In contrast, the TORKinib PP242 (*65*), which inhibits both mTOR complexes, reduced the abundance of mTOR-pS^{2481} in a dose-dependent manner (Fig. 1, C and E), which is consistent with results obtained with Torin1, another TORKinib (*64*, *66*). Therefore, our results suggest that mTOR-pS^{2481} is reduced by mTORC2, but not by mTORC1 inactivation.

Because there are rapamycin-insensitive mTORC1 functions (*67*), we also knocked down specific mTORC1 and mTORC2 components to assess the dependence of mTOR-pS^{2481} on the activity of the two complexes. When the mTORC1-specific component Raptor was knocked down, mTOR-pS^{2481} was unchanged (Fig. 1F), whereas there was a significant reduction in mTOR-pS^{2481} by 67% (three independent experiments, SEM 8%) when the mTORC2-specific component Rictor was knocked down (representative experiment shown in Fig. 1G). Thus, both knockdown and pharmacological experiments indicated that mTOR-pS^{2481} serves as an mTORC2-specific readout in our system.

Parameterization of the network model

To parameterize the static network model, we generated semiquantitative dynamic phosphorylation immunoblot data for network components along the signaling cascade (Fig. 1A). We analyzed HeLa cells under starvation conditions, meaning that they were deprived of amino acids and growth factors for 16 hours to fully inhibit mTOR network activity, and also cells that had been starved and then stimulated with aa/insulin to assure full induction of both mTOR complexes. Dynamics of the mTOR network were monitored from 1 min up to 2 hours after induction with aa/insulin (Fig. 2A). Signals were quantitatively analyzed (see Materials

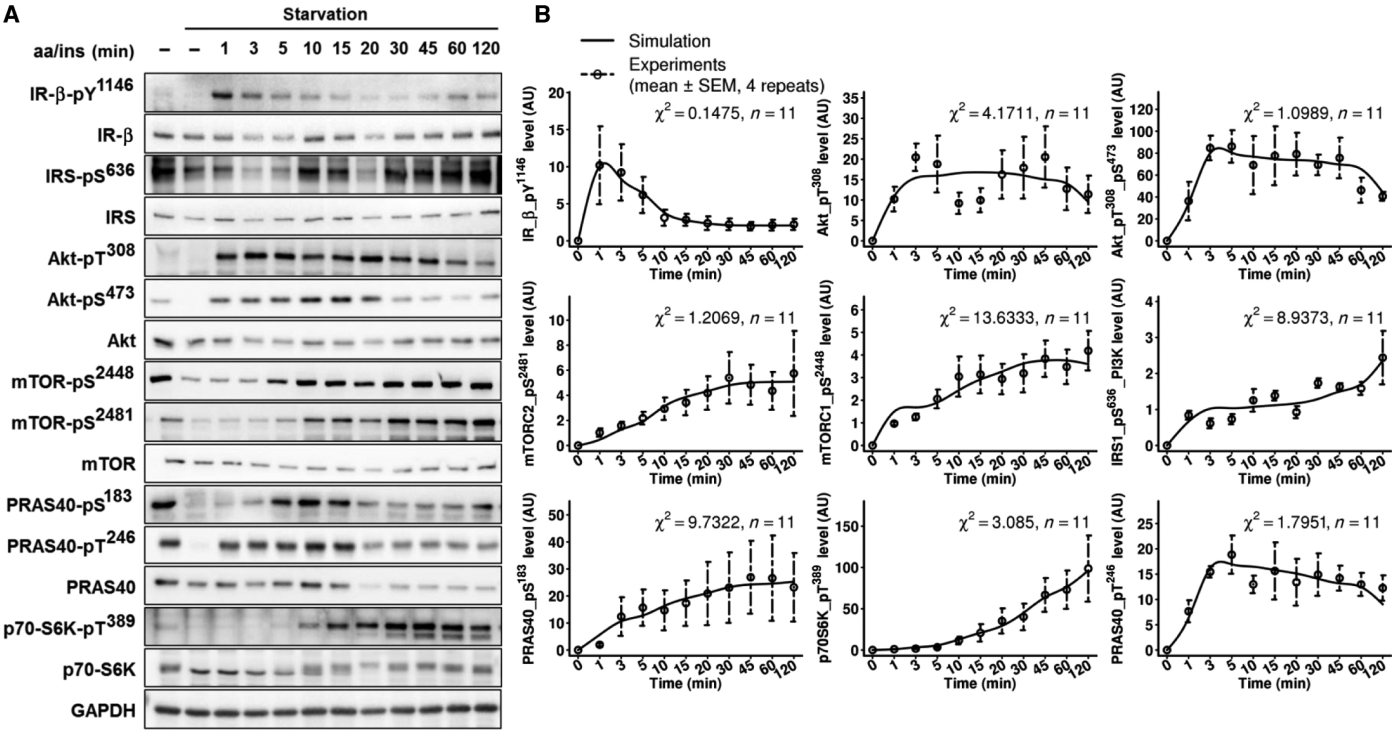

Fig. 2. Setup of a dynamic insulin/mTOR network model. (A) Dynamic quantitative time course acquisition. mTOR pathway activation was followed over time by measuring phosphorylation dynamics of central network components. A representative experiment is shown; signal intensities were quantified and descriptive statistics were computed over four replicates. (B) Comparison between the simulated time courses of the general model (solid lines) and the experimental time courses (points, dotted error bars) within [0, 120] min. For each curve, the χ^2 computed over n time points is reported as goodness-of-fit measure.

and Methods). Because signal linearities are critical for quantitative data generation (*68*), we confirmed the linear signal–to–protein amount relationships by detection of serial dilutions of whole-cell lysates (fig. S2). We calibrated the model parameters by means of the experimental mean time courses (Fig. 2B).

The initial concentrations of the species in their nonphosphorylated state were determined directly from our semiquantitative data (see Materials and Methods). For all other species, the initial concentrations were set to 0. Because it is difficult to fit large numbers of parameters to data to estimate kinetic rate constants (*69*–*71*), which are necessary to calibrate the model, we divided the data fitting into calibration phases and resolved each phase with an iterative procedure (figs. S3 and S4). This procedure is summarized by the following steps: (i) The initial values of the parameters that needed optimization were assigned by random generation. (ii) The calibration was repeated until a set of parameters with consistent values was identified. (iii) This set of parameters was fixed and the remaining free parameters were calibrated again by repeating the process. In phase 1 of the estimation of kinetic rate constants, we sought to identify isolated modules that could be calibrated independently within the network. Because IR regulation was not affected by the rest of the network, this module could be isolated and we could calibrate three parameters at once: the kinetics of IR activation by insulin, dephosphorylation to a refractory state, and transition to a receptive state. We initially generated a model that was independent of the pathway by which mTORC2 was activated. We temporarily modeled the regulation of the mTORC2 substrate Akt-S^{473} and mTORC2 component mTOR-S^{2481} with two autoactivation mechanisms, which were then calibrated with the Akt-pS^{473} and mTOR-pS^{2481} experimental data sets. This enabled us to reproduce Akt-pS^{473} activation while maintaining mTORC2 isolated from the network. During phase 2, a total of 24 reaction rate constants were estimated with eight experimental readouts. Finally, in phase 3, we replaced the autoactivation mechanism of Akt-pS^{473} with a phosphorylation mediated by mTORC2-pS^{2481}. Because the initial induction of Akt-pS^{473} occurred before mTOR-pS^{2481} was induced (Fig. 2, A and B), mTORC2-pS^{2481} alone could not reproduce the dynamics of the experimental data for Akt-pS^{473}. mTORC2 is not the only PDK2 candidate that may phosphorylate Akt-S^{473}; therefore, we introduced an additional PDK2 species and recalibrated the phosphorylation of Akt-S^{473} under the influence of the two kinases. In this phase, three kinetic rate constants were estimated with the Akt-pS^{473} experimental data.

Once this process of parameterization was complete, the experimental and simulated time courses matched well for all the analyzed mTOR network readouts (Fig. 2B). The ordinary differential equations (ODEs) and estimated parameters for the general model are provided in tables S1 and S2. Identifiability analysis, which indicates whether the parameters can be estimated with confidence from the available data, and sensitivity analysis, which indicates how sensitive model behavior is to variation in each parameter, for the general model are shown in figs. S5 and S6. The identifiability analysis does not show high correlation between estimated parameters, indicating that they can be identified.

Validation of the mTORC1 branch: Network perturbation by gradual mTORC1 inhibition

If the parameterized model correctly represents the biological mTOR network dynamics in response to aa/insulin, model simulations must

accurately reflect the dynamics of known network responses to a gradual perturbation. To validate the mTORC1 branch of the model, we perturbed the network by gradually inhibiting mTORC1 first in silico and then experimentally with an inducible Raptor knockdown (shRaptor) cell line. The model was used to simulate the effect of gradual mTORC1 inhibition on the activation dynamics of the direct mTORC1 substrate p70-S6K-pT^{389} at several time points after induction with aa/insulin. The model predicted a constant increase in p70-S6K-pT^{389} signal from 10 min to 2 hours after induction. Furthermore, the model also predicted that p70-S6K-pT^{389} would decrease starting 10 min after induction in a near-linear manner in response to gradual Raptor (mTORC1) inhibition, whereas there should be no detectable increase or Raptor-dependent change in p70-S6K-pT^{389} below 5 min after induction (Fig. 3A). We tested the predicted quantitative p70-S6K-pT^{389} response upon gradual mTORC1 inhibition (Fig. 3B) at specific time points (indicated in the simulation in Fig. 3A by the green lines) and found that the dynamic simulations for p70-S6K-pT^{389} were validated by our experimental data (Fig. 3, C and D). Both the simulations (Fig. 3B) and the experimental results (Fig. 3D) for the change in p70-S6K-pT^{389} in response to gradual Raptor inhibition at 20 and 45 min after induction with aa/insulin matched, showing an overall increase in signal at 45 min after induction and no signal at 3 min after induction.

Hence, we confirmed that the model accurately simulated the dynamic behavior of the mTORC1 substrate p70-S6K-T^{389} in response to aa/insulin and to a network perturbation (Raptor inhibition). This was performed with an experimental perturbation that was not used for parameterization.

Exploration of alternative network structures: Regulation of mTORC2 by the TSC1-TSC2 complex

The mechanism by which TSC1-TSC2 influences mTORC2 activity is currently unclear, with both a direct activation of mTORC2 by TSC1-TSC2 and an indirect effect of the TSC1-TSC2 through mTORC1 and the NFL suggested (*31*, *33*, *35*). The evidence for these mechanisms involves experimental designs that could affect the system in a manner that could complicate the interpretation, for example, overexpression of NFL-independent PI3K versions (*31*) or TSC2 ablation in combination with subsequent in vitro mTOR kinase assays (*33*).

To establish an approach with minimal complicating manipulations, we applied a combined experimental-computational strategy. Because the different suggested molecular mechanisms by which TSC1-TSC2 regulates mTORC2 should result in mechanism-specific changes in the dynamics of the mTORC2 readouts, the response of the readouts to network perturbations should be predictable and distinguishable by our dynamic network model. On the basis of the existing literature, we postulated three different hypotheses for the molecular connection or lack thereof between TSC1-TSC2 and mTORC2 (Fig. 4A). (Hypothesis 1) TSC-dependent: TSC1-TSC2 directly activates mTORC2 in response to insulin and has opposite effects on mTORC1 and mTORC2. (Hypothesis 2) NFL-dependent: mTORC2 is activated by insulin through PI3K, but independently of Akt and TSC1-TSC2; however, mTORC2 activity can be inhibited indirectly by TSC1-TSC2 ablation through NFL-mediated inhibition of PI3K. (Hypothesis 3) PI3K-independent: mTORC2 is activated by insulin in a manner that is independent of both TSC1-TSC2 and PI3K.

We translated these three alternative modes of mTORC2 regulation into the corresponding network structures, reusing the same kinetic parameters of our previous model (Fig. 4B). To keep the hypotheses as comparable as possible, each hypothesis shared the network topology of the general model but assumed a specific mTORC2 upstream regulator (Fig. 4B). We adopted the following rationale: Let M be a model fitting some data and S a species in M. If a modifier (F) directly upstream of S is selected and recalibration solely of the dynamics of S maintains a close fit between the simulated time course for S and the experimental data for S, then all time course curves downstream of S will continue to fit their corresponding data. The model output,

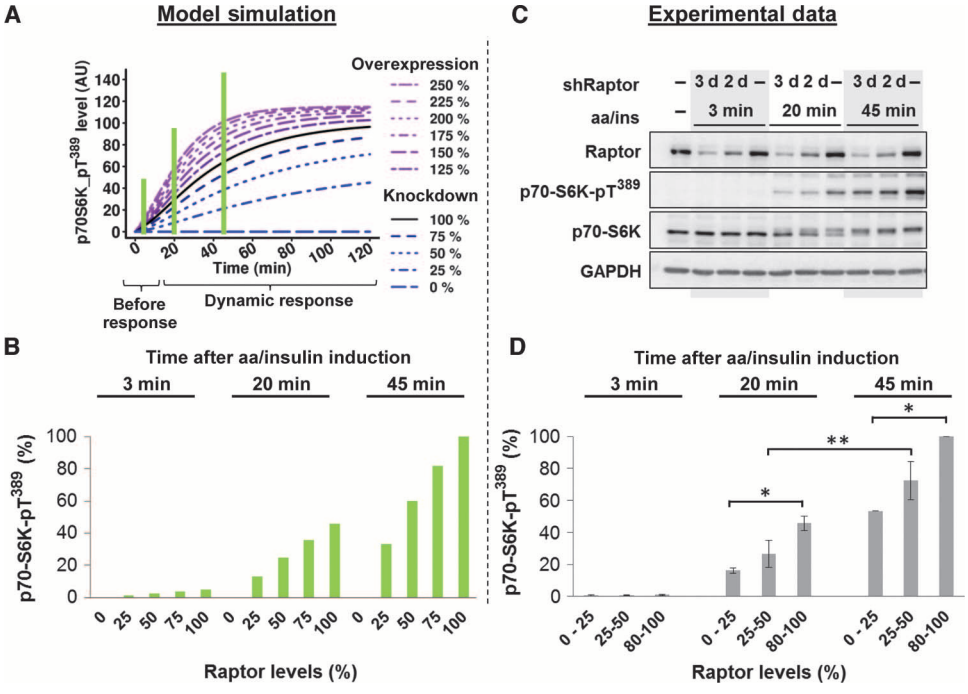

Fig. 3. Validation: dynamic response of p70-S6K-pT^{389} to gradual Raptor inhibition. (A) Model predictions for p70-S6K-pT^{389} dynamics in response to a perturbation of mTORC1. The curves show the simulated response to gradual mTORC1 inhibition starting at 5 to 10 min after induction with aa/insulin. The model was simulated with both mTORC1 overexpression and knockdown conditions. Time points for experimental validation are indicated by green lines. (B) Simulated and quantified relative amounts of p70-S6K-pT^{389} under conditions of mTORC1 reduction (0, 25, 50, 75, and 100%) at selected time points after induction with aa/insulin. (C) Experimental validation of the effect of gradual Raptor knockdown (shRaptor) on p70-S6K phosphorylation in starved cells induced with aa/ins for the indicated times. Data are representative of three experiments. d, days. (D) Experimentally determined and quantified p70-S6K-pT^{389} amounts at the indicated times after induction with aa/insulin in cells in which Raptor was knocked down. Data are the average and SEM of three experiments. *P < 0.05; **P < 0.01; low Raptor levels compared to high Raptor levels after 20- and 45-min induction; 20- compared to 45-min induction. Differences in p70-S6K-pT^{389} were significant. aa/ins, aa/insulin.

however, after perturbation of F will not necessarily maintain a fit with the corresponding data when the introduced upstream connection is incorrect.

We defined three new models in which the network and the parameters of our previous model were maintained and only the mTORC2 kinetics were reestimated according to each hypothesis (tables S1 and S3). The

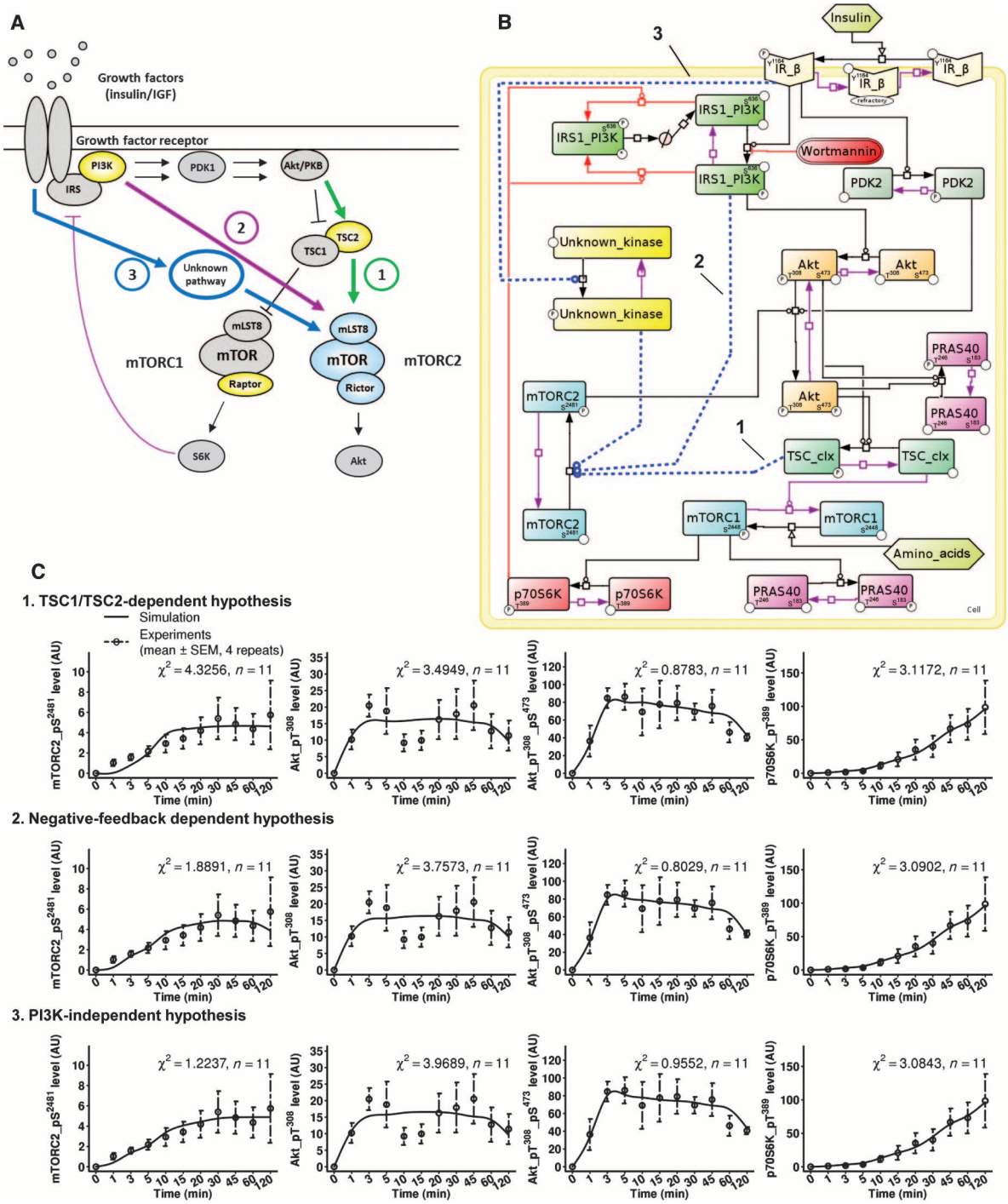

Fig. 4. Three hypotheses for mTORC2 regulation by insulin. (A) Schematic representation of the insulin-induced mTORC1-mTORC2 pathway with three different hypotheses (1, green; 2, purple; 3, dark blue) for mTORC2 activation. Network components that were targeted for perturbations are highlighted in yellow. (B) Reduced graphical network model including the three hypotheses (1, 2, and 3, indicated by the dotted lines), translated into different network structures. (C) Comparisons of simulated time courses, calibrated for each hypothesis, with experimental data. Data are for mTORC2 readouts (mTOR-pS^{2481}, Akt-pS^{473}), the PI3K readout Akt-pT^{308}, and the mTORC1 readout p70-S6K-pT^{389} (see fig. S7 for curves of all other readouts).

total goodness of fit for the general model and each hypothesis showed that no model could be statistically rejected (table S4). For each hypothesis, we performed time course simulations and experimental validation for the mTORC2 readouts mTOR-pS^{2481} and Akt-pS^{473}, the PI3K readout Akt-pT^{308}, and the mTORC1 substrate p70-S6K-pT^{389} (Fig. 4C). The curves for all other analyzed network components are provided in fig. S7. The simulations matched the experimental time courses, indicating that the hypotheses were compatible with the observed dynamics for mTORC2 activation and more generally for the mTOR signaling network. Identifiability and sensitivity analyses for the three models representing each hypothesis are shown in figs. S8 to S13.

We next introduced gradual network perturbations that prevented either TSC1-TSC2 activity (TSC1-TSC2 inhibition), the NFL (mTORC1 inhibition), or insulin activation of the mTOR complexes (PI3K inhibition). For each of the three perturbations and each of the three hypotheses, we modeled the dynamic network response of the readouts of mTORC2 activity (Fig. 5), of mTORC1 activity (fig. S14), and of PI3K activity (fig. S15).

Experimental testing: TSC2-independent mTORC2 induction

From the information obtained from the alternative simulations, we identified experimental setups and time points after induction with aa/insulin for the mTORC2 readouts (mTOR-pS^{2481}, Akt-pS^{473}) that would specifically distinguish among hypotheses 1, 2, and 3 (green lines in Fig. 5). These predictions were then tested experimentally (Figs. 6 to 8).

The models predicted that for gradual TSC1-TSC2 inhibition, if hypothesis 1 was correct, then the abundance of mTOR-pS^{2481} would be affected by TSC1-TSC2 inhibition in a near-linear manner down to minimum levels (Fig. 5A). In contrast, for hypothesis 2, simulated mTOR-pS^{2481} dynamics were only slightly affected by TSC1-TSC2 inhibition, and for hypothesis 3, mTOR-pS^{2481} was not affected (Fig. 5A). For Akt-pS^{473} dynamics, if hypothesis 2 or 3 is correct, then Akt-pS^{473} should only be weakly affected 5 min after induction and should exhibit a gradual decrease starting 10 min after induction for the rest of the time course (Fig. 5B). For hypothesis 1, the model predicted a stronger reduction of Akt-pS^{473} in response to TSC1-TSC2

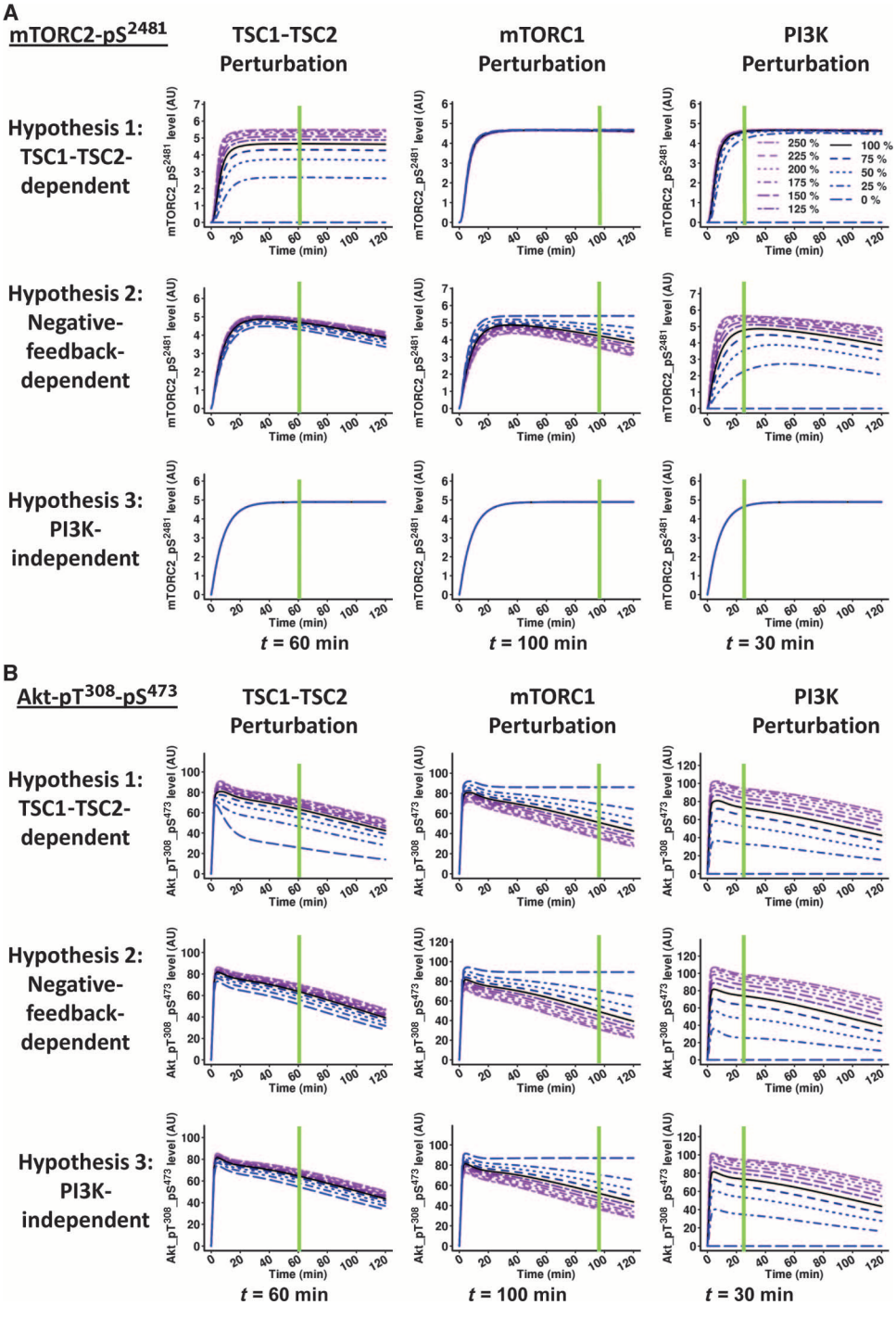

Fig. 5. Simulations of network perturbations at several levels within the network and differential dynamic network responses for the three different hypotheses. (**A**) Simulated mTOR-pS^{2481} response upon aa/insulin induction upon the indicated perturbations: TSC1-TSC2 (experimental equivalent: gradual TSC2 knockdown), mTORC1 (experimental equivalent: gradual Raptor knockdown), and PI3K (experimental equivalent: gradual PI3K inhibition with wortmannin) for hypotheses 1, 2, and 3. The time points that were experimentally tested are indicated with green lines. (**B**) Simulated Akt-pT^{308}-pS^{473} response for each of the three hypotheses upon aa/insulin induction upon perturbations of TSC1-TSC2, mTORC1, and PI3K. The time points that were experimentally tested are indicated with green lines.

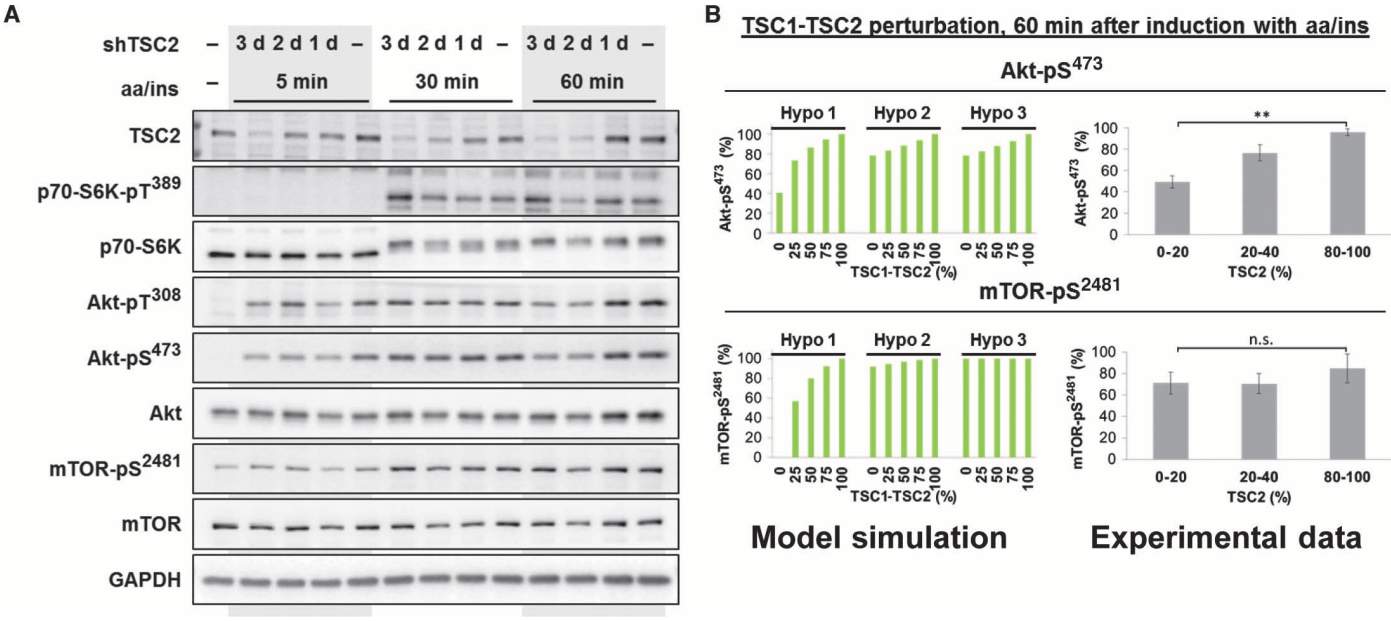

Fig. 6. mTOR-pS^{2481} is not directly activated by TSC1-TSC2. mTOR-pS^{2481} is not directly activated by TSC1-TSC2. (**A**) Representative immunoblot results of the network response upon mTOR network activation in cells in which TSC2 was knocked down for the indicated amounts of time. Data are representative of three experiments. d, days. (**B**) Quantitative representations of simulated and experimentally determined Akt-pS^{473} and mTOR-pS^{2481} dynamics 60 min after induction with aa/ins in response to a gradual TSC2 knockdown. (Left) Relative quantitations of the simulated Akt-pS^{473} and mTOR-pS^{2481} behavior for the three hypotheses (Hypo 1, 2, and 3) upon gradual TSC2 knockdown. The amount of TSC1-TSC2 is indicated as a percentage of the total in the control system in the absence of knockdown. (Right) Quantitations of experimental results for 60 min after induction with aa/ins in cells in which TSC2 was reduced to the indicated amounts (percent of total). Values from three independent experiments were merged and grouped according to the amount of TSC2. $^{**}P < 0.01$; n.s., not significant; low TSC2 levels compared to high TSC2 levels. Differences were significant for Akt-pS^{473} and not significant for mTOR-pS^{2481}.

inhibition at all time points after induction, compared to the reduction predicted for hypothesis 2 or 3. Thus, these simulation results indicated that observation of mTOR-pS^{2481} in response to gradual TSC1-TSC2 inhibition should effectively distinguish hypothesis 1 from the other two hypotheses.

For experimental testing, we generated an inducible short hairpin TSC2 (shTSC2) cell line and induced TSC2 knockdown for 0, 1, 2, or 3 days, which resulted in a gradual decline in the amount of TSC2 (Fig. 6A). After starvation, cells were stimulated with aa/insulin for 5, 30, and 60 min. Because TSC1-TSC2 is a negative regulator of mTORC1, p70-S6K-pT^{389} increased as expected with gradual TSC2 inhibition (Fig. 6A). Relative quantitations for Akt-pS^{473} and mTOR-pS^{2481} at 60 min after aa/insulin induction are shown for the simulations of the three hypotheses and for the experimental data (Fig. 6B). Both the time course analysis (Fig. 6A) and the analysis of the effect of increasing knockdown of TSC2 (Fig. 6B) on Akt-pS^{473} suggested that hypothesis 2 or 3 may be correct. Hypothesis 1 of direct TSC1/2 activation of mTORC2 was clearly excluded because mTOR-pS^{2481} was unaffected by TSC2 inhibition at all time points (Fig. 6A) and at all amounts of TSC1-TSC2 inhibition (Fig. 6B). Our experimental data are in line with reported findings, indicating that TSC1-TSC2 does affect Akt-pS^{473} (*31*, *33*, *35*). However, according to our simulations, the regulation of Akt-pS^{473} by TSC1-TSC2 depends on the NFL and PI3K and, thus, in the absence of TSC1-TSC2 mTORC2–mediated phosphorylation of AktS^{473} is indirectly inhibited. Because the direct mTORC2 readout mTOR-pS^{2481} was unchanged in the absence of TSC1-TSC2, we can rule out TSC1-TSC2 as a direct activator of mTORC2.

We followed the same procedure that we used to identify the best experimental condition to assess whether TSC1-TSC2 indirectly controls mTORC2 through the NFL (*35*) (hypothesis 2). For gradual mTORC1 inhibition and consequent NFL inhibition, all three model structures predicted an increase of Akt-pS^{473} with decreasing mTORC1 activity (Fig. 5B). The simulations also predicted that mTOR-pS^{2481}would remain unaffected in hypotheses 1 and 3 and would gradually increase in response to mTORC1 inhibition in hypothesis 2 starting 40 min after induction with aa/insulin. This effect should be clearly experimentally visible at 100 min after induction with aa/insulin, and this paradigm could be used to distinguish hypothesis 2 from the other hypotheses.

For experimental testing, the specific mTORC1 component Raptor was gradually inhibited by knocking down Raptor in an inducible shRaptor cell line for 0, 1, 2, or 3 days. Cells were starved and stimulated with aa/insulin for 45, 100, and 180 min (Fig. 7A). Verification of effective mTORC1 inhibition in this experimental setup was performed by monitoring the abundance of p70-S6K-pT^{389}, which showed the expected reduction in response to decreased Raptor (Fig. 3, B and D). Relative quantitations of Akt-pS^{473} and mTOR-pS^{2481} in response to gradual Raptor inhibition are shown for the simulations of the three hypotheses and for experimental data at 100 min after induction with aa/insulin (Fig. 7B). As predicted for all three hypotheses, Akt-pS^{473} showed a significant increase with declining Raptor levels because the NFL is inhibited (Fig. 7, A and B). The abundance of Akt-pT^{308} also increased as mTORC1 was inhibited (Fig. 7A). In contrast, mTOR-pS^{2481} remained unaffected at all time points after induction with aa/insulin and at all Raptor levels (Fig. 7, A and B), which

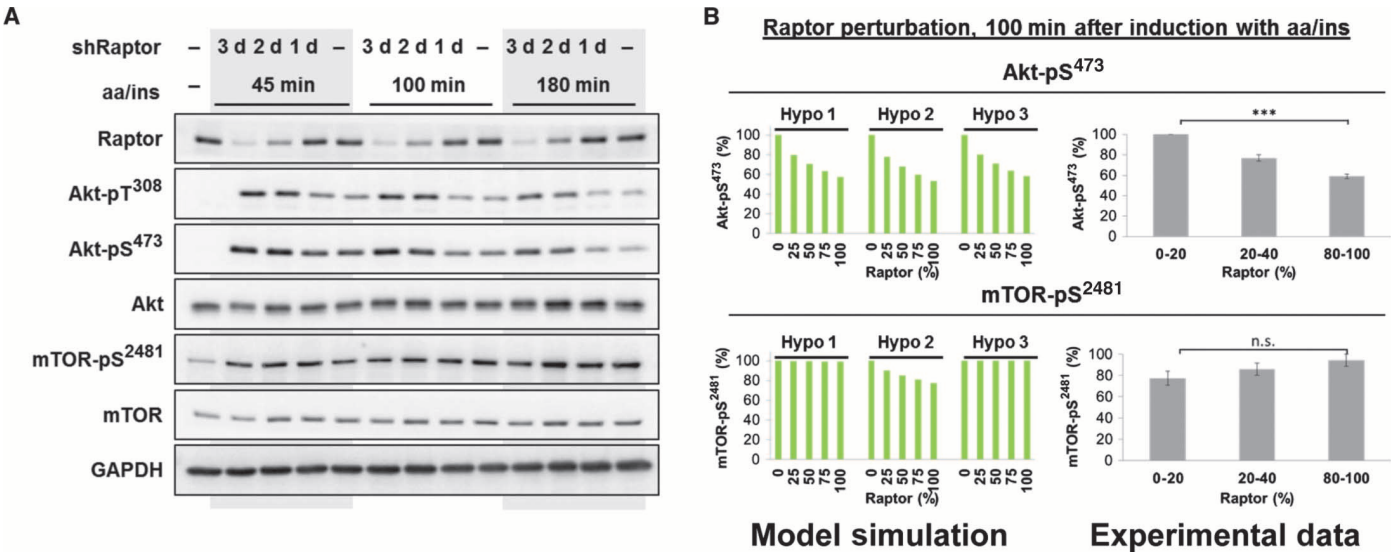

Fig. 7. mTOR-pS^{2481} is not affected by the NFL. (**A**) Representative immunoblot results of the network response upon mTOR network activation in cells in which Raptor was knocked down for the indicated amounts of time. Data are representative of three experiments. d, days. (**B**) Quantitative representations of simulated and experimentally determined Akt-pS^{473} and mTOR-pS^{2481} dynamics 100 min after induction with aa/ins in response to knockdown of Raptor to the indicated amounts (percent of total in the absence of knockdown). (Left) Relative quantitations of the simulated Akt-pS^{473} and mTOR-pS^{2481} behavior for the three hypotheses (Hypo 1, 2, 3) upon a gradual Raptor knockdown. (Right) Quantitations of experimental results 100 min after induction with aa/ins in cells in which Raptor was knocked down to the indicated amounts (percent of total). Values from three independent experiments were merged and grouped according to the amount of Raptor. Data are the average and SEM. ***$P < 0.001$; n.s., not significant; low Raptor levels compared to high Raptor levels. Differences were significant for Akt-pS^{473} and not significant for mTOR-pS^{2481}.

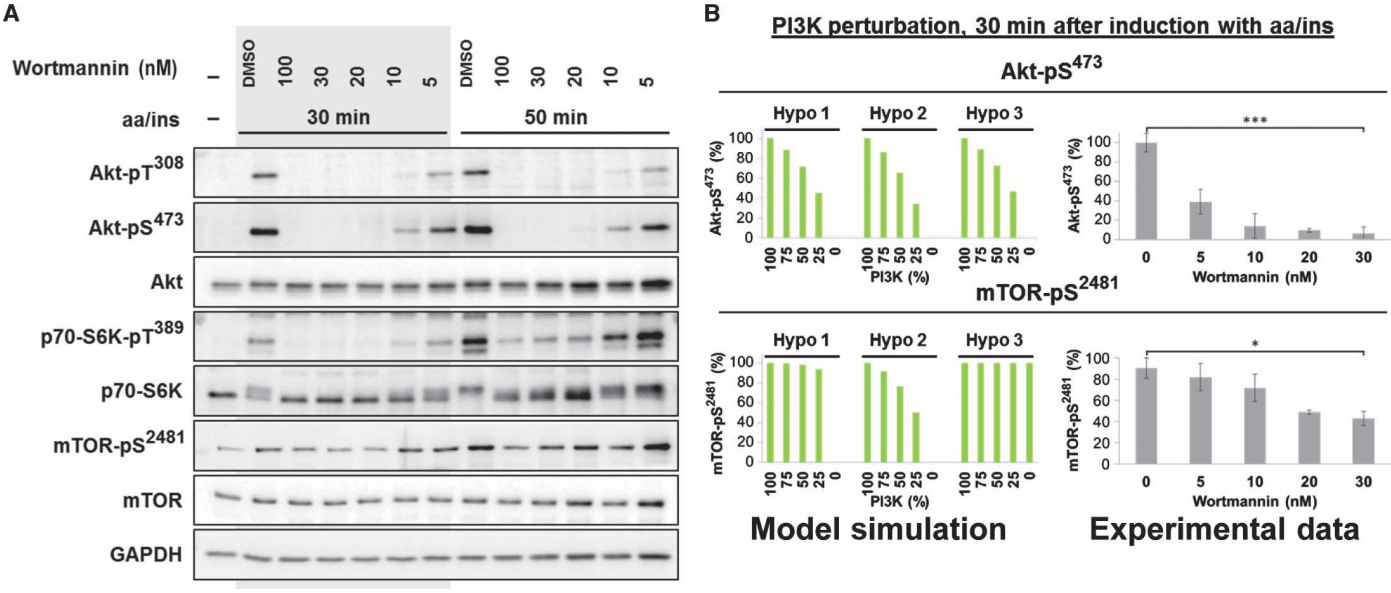

Fig. 8. mTOR-pS^{2481} is sensitive to the PI3K inhibitor wortmannin. (**A**) Representative immunoblot results of the network response upon mTOR network activation with aa/ins in the presence of wortmannin to inhibit PI3K. Data are representative of three experiments. (**B**) Quantitative representations of simulated and experimentally determined Akt-pS^{473} and mTOR-pS^{2481} dynamics 30 min after induction with aa/ins in cells in which PI3K activity was inhibited to the indicated amount (percent of total activity). (Left) Relative quantitations of the simulated Akt-pS^{473} and mTOR-pS^{2481} behavior for the three hypotheses (Hypo 1, 2, 3) in response to gradual PI3K inhibition (percent of total activity). (Right) Quantitations of experimental results 30 min after induction with aa/ins in cells in which PI3K was inhibited with the indicated concentrations of wortmannin. Data are the average and SEM of three experiments. *$P < 0.05$; ***$P < 0.001$; 30 nM compared to 0 nM wortmannin. Differences were significant for both Akt-pS^{473} and mTOR-pS^{2481}.

excludes hypothesis 2. Therefore, our model and the experimental testings allowed us to exclude the previously suggested hypothesis of an indirect mTORC2 regulation by TSC1-TSC2 and the NFL. Hence, mTORC2 is neither directly nor indirectly regulated by TSC1-TSC2.

Having excluded both hypotheses 1 and 2 and established that mTORC2 induction was independent of the NFL that inhibits IRS1 and thus PI3K activity, we directly tested whether the model and experimental testing would confirm hypothesis 3, that PI3K inhibition would not affect mTOR-pS^{2481} induction by aa/insulin. For gradual PI3K inhibition, our simulations predicted that Akt-pS^{473} in all three hypotheses would be reduced to a minimum level at all time points after induction with aa/insulin (Fig. 5B). In contrast, the model predicted that mTOR-pS^{2481} (Fig. 5A) would remain either unaffected by PI3K inhibition (hypotheses 1 and 3) or decline with decreasing PI3K starting 20 min after induction (hypothesis 2). Because hypotheses 1 and 2 were already excluded, we expected PI3K inhibition to result in the mTOR-pS^{2481} behavior predicted by hypothesis 3.

To experimentally test the validity of hypothesis 3, we starved cells, gradually inhibited PI3K with increasing wortmannin concentrations, and induced mTOR signaling by aa/insulin for 30 and 50 min (Fig. 8A). We chose a maximal wortmannin concentration of 100 nM, at and below which this inhibitor is specific for class I PI3Ks (*72*). Quantification of simulated and experimentally measured Akt-pS^{473} and mTOR-pS^{2481} in response to gradual PI3K inhibition is shown for 30 min after induction with aa/insulin (Fig. 8B). In agreement with our model, the dynamics of Akt-pS^{473} closely resembled the PDK1 phosphorylation of Akt-T^{308}, decreasing as PI3K was inhibited (Fig. 8A). The mTORC1 target p70-S6K-pT^{389} behaved similarly (Fig. 8A). In line with the literature (*73*) and as predicted by all three hypotheses, Akt-pS^{473} was already inhibited at 5 nM wortmannin and was strongly inhibited by concentrations of 10 nM wortmannin or higher (Fig. 8, A and B). Surprisingly, mTOR-pS^{2481} also was inhibited by wortmannin concentrations of 20 nM or higher (Fig. 8, A and B). Thus, our model and the experimental testing also exclude hypothesis 3 because mTORC2 activation appears to depend on PI3K activity.

A novel network structure integrating PI3K-dependent and NFL-independent activation of mTORC2

Our combined experimental-computational approach showed that insulin regulates mTORC2 through a wortmannin-sensitive enzyme (likely PI3K), and that mTORC2 is affected neither by the NFL nor by TSC1-TSC2. We, therefore, had to postulate a hypothesis 4: There is another kinase, in particular a wortmannin-sensitive but IRS1-independent PI3K species, that is activated by the IR and stimulates mTORC2 in response to insulin (Fig. 9, A and B). The model did not require recalibration because the new branch for mTORC2 activation by insulin was similar to the PI3K-independent hypothesis 3 but contained the new proposed PI3K, which is sensitive to wortmannin and refractory to the NFL.

We experimentally verified that this hypothesis 4 model fitted the data by showing that the simulated time courses matched the experimental readout dynamics [Fig. 9C (mTOR-pS^{2481} and Akt-pS^{473}) and fig. S16A

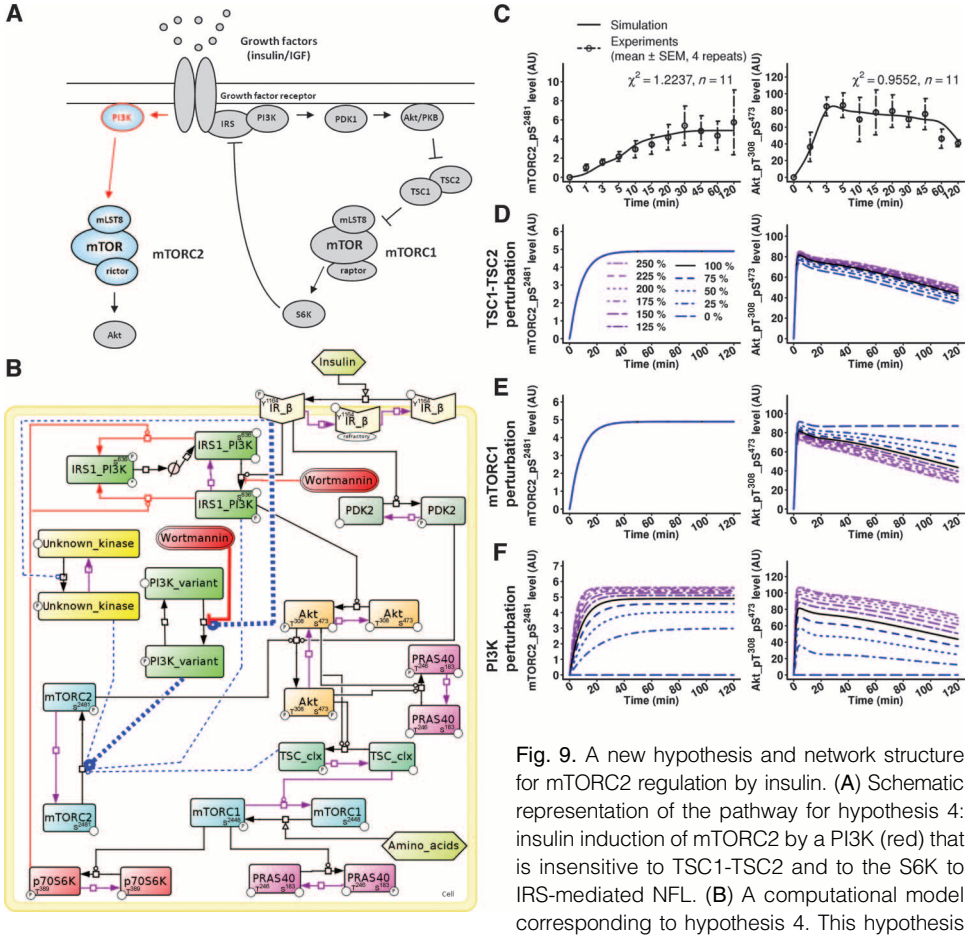

Fig. 9. A new hypothesis and network structure for mTORC2 regulation by insulin. (**A**) Schematic representation of the pathway for hypothesis 4: insulin induction of mTORC2 by a PI3K (red) that is insensitive to TSC1-TSC2 and to the S6K to IRS-mediated NFL. (**B**) A computational model corresponding to hypothesis 4. This hypothesis was equivalent to hypothesis 3 (PI3K and TSC1-TSC2–independent activation), assuming that the mTORC2 activator was sensitive to wortmannin. (**C**) The model simulation data for hypothesis 4 match the experimental dynamic phosphorylation data. The simulated and experimentally measured dynamics are shown for the mTORC2 readouts mTOR-pS^{2481} and Akt-pS^{473} (see fig. S16 for all other readouts). (**D**) Predictions for mTOR-pS^{2481} and Akt-pS^{473} upon gradual TSC1-TSC2 knockdown match the experimental data, which are presented in Fig. 6, A and B (right side). Whereas at 60 min after induction Akt-pS^{473} is gradually reduced by TSC2 inhibition, mTOR-pS^{2481} is TSC2-insensitive. See fig. S16 for Akt-pT^{308} and p70-S6K-pT^{389}. (**E**) Predictions for mTOR-pS^{2481} and Akt-pS^{473} readouts upon gradual Raptor knockdown match the experimental data, which are presented in Fig. 7, A and B (right side). Whereas at 100 min after induction Akt-pS^{473} is gradually induced by Raptor inhibition, mTOR-pS^{2481} is Raptor-insensitive. See fig. S16 for Akt-pT^{308} and p70-S6K-pT^{389}. (**F**) Predictions for mTOR-pS^{2481} and Akt-pS^{473} readouts upon gradual PI3K inhibition match the experimental data, which are presented in Fig. 8, A and B (right side). Both Akt-pS^{473} and mTOR-pS^{2481} are gradually reduced by wortmannin at 30 min after induction. See fig. S16 for Akt-pT^{308} and p70-S6K-pT^{389}.

(curves for all other readouts)]. Next, we modeled the dynamic network response under all previously tested network perturbations (gradual TSC1-TSC2, mTORC1, or PI3K inhibition) and compared the simulations to our experimental data (simulation in Fig. 9, D to F, and fig. S16B; data in Figs. 6 to 8). For each of the three network perturbations, the predictions for all readout dynamics (Fig. 9, D to F) matched the experimental data (Figs. 6 to 8). Identifiability and sensitivity analyses for hypothesis 4 are shown in figs. S17 and S18. The identifiability analysis reports low correlation between the estimated parameters, indicating that the parameters can be identified. Thus, the new network model of a PI3K-species–dependent and NFL-independent mTORC2 induction accurately predicted the responsiveness of mTORC2 to PI3K inhibition, and mTORC2 insensitivity to gradual TSC1-TSC2 or mTORC1 inhibition.

Because a model for mTORC2 activation through an NFL-insensitive PI3K was unexpected, we performed additional experimental testing. To confirm that the reduction of mTOR-pS^{2481} in response to wortmannin was associated with mTORC2, we treated cells with PP242 or wortmannin, or knocked down Raptor and then immunoprecipitated mTORC2 with an antibody recognizing Sin1 (Fig. 10A). We found that both PP242 and wortmannin significantly reduced mTOR-pS^{2481} associated with the immunoprecipitated mTORC2 (Fig. 10B), but that mTORC1 inhibition by shRaptor did not affect mTOR-pS^{2481} associated with the immunoprecipitated mTORC2 (Fig. 10, A and B). These results are consistent with the whole-cell lysate experiments (Figs. 1, E and F, and 8B) and support our previous conclusion that wortmannin inhibits mTORC2.

To verify the PI3K specificity of the wortmannin effect on mTORC2, we inhibited PI3K by two alternative means—with another PI3K inhibitor LY294002 or by overexpression of the PI3K antagonist PTEN (phosphatase and tensin homolog deleted from chromosome 10). We found that mTOR-pS^{2481} was reduced in cells exposed to LY294002 at concentrations as low as 1 μM (Fig. 10C) and in cells overexpressing PTEN (Fig. 10D). Thus, three separate experimental approaches indicated that mTORC2 activation depends on PI3K.

Mechanistic exploration in several cell types: mTORC2 activation independent of Akt

The hypothesis 4 model predicted that the PI3K-dependent, NFL-insensitive activation of mTORC2 should be insensitive to Akt. We overexpressed myristoylated Akt (myr-Akt), which is constitutively recruited to the membrane and constitutively active even without insulin (*74*), or a kinase-dead myr-Akt variant (myr-Akt K179M) in HeLa and C2C12 cells and monitored the activity of mTORC1 and mTORC2 (Fig. 10, E and F). For cells expressing the constitutively active Akt, phosphorylation of the mTORC1 substrate p70-S6K-T^{389} was increased by myr-Akt, whereas it was decreased in the cells expressing the myr-Akt K179M. In contrast, the mTORC2 readout mTOR-pS^{2481} was unchanged in the presence of either of the two myr-Akt constructs. We confirmed that mTOR-pS^{2481} specifically reflected mTORC2 activity in C2C12 cells because the amount of mTOR-pS^{2481} was decreased in response to the mTOR kinase inhibitor PP242, but was unaffected by the mTORC1-specific

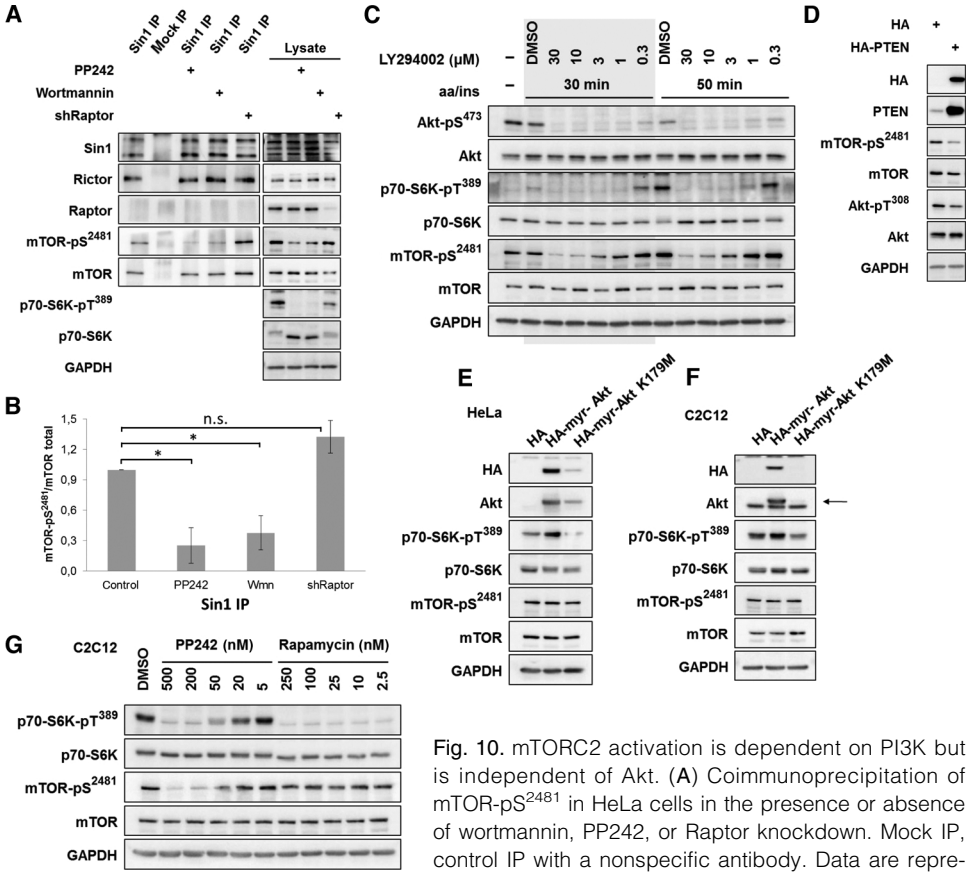

Fig. 10. mTORC2 activation is dependent on PI3K but is independent of Akt. (**A**) Coimmunoprecipitation of mTOR-pS^{2481} in HeLa cells in the presence or absence of wortmannin, PP242, or Raptor knockdown. Mock IP, control IP with a nonspecific antibody. Data are representative of three experiments. (**B**) Quantitation of data from three experiments similar to that shown in (A) for mTOR-pS^{2481} relative to total amount of immunoprecipitated mTOR. *$P < 0.05$; n.s., not significant. For PP242 and wortmannin treatments compared to control, there were significant differences in mTOR-S^{2481} association with Sin1. For the Raptor knockdown compared to control, the differences in mTOR-pS^{2481} association were not significant. (**C**) Effect of the PI3K inhibitor LY294002 on mTOR-pS^{2481} and other components of the mTOR network in HeLa cells. Data are representative of three experiments. (**D**) Effect of HA-tagged PTEN overexpression on mTOR-pS^{2481}. Data are representative of three experiments. HA, HeLa cells transfected with empty vector control. (**E**) Effect of constitutively active (HA–myr-Akt) or kinase-dead (HA–myr-Akt K179M) Akt on mTOR-pS^{2481} and other components of the mTOR network in HeLa cells. Data are representative of three experiments. (**F**) The effect of constitutively active (HA–myr-Akt) or kinase-dead (HA–myr-Akt K179M) Akt on mTOR-pS^{2481} and other components of the mTOR network in C2C12 myoblasts. The specific Akt signal is indicated by an arrow. Data are representative of three experiments. (**G**) Confirmation that mTOR-pS^{2481} is a specific mTORC2 readout in C2C12 myoblasts. The indicated proteins were detected in cells in the presence or absence of the indicated concentrations of PP242 or rapamycin in the continuous presence of aa/insulin. Data are representative of three experiments.

drug rapamycin (Fig. 10G). Thus, mTORC2 activity was not induced by Akt.

DISCUSSION

We present a dynamic mTOR network model, which is based on an integrated experimental-computational approach. We initially postulated three different network structures for mTORC2 induction by insulin, which guided experiments to test the hypotheses. The results of the simulations and experimental data indicated that none of the previously suggested mechanisms of mTORC2 activation were accurate: TSC1-TSC2 is not a direct activator of mTORC2; TSC1-TSC2 does also not indirectly control mTORC2 through inhibition of PI3K by the NFL; and mTORC2 activation depends on PI3K. However, the PI3K-dependent mTORC2 activation is insensitive to the NFL. We, therefore, postulated an activation pathway involving a PI3K variant that is independent of the NFL and we tested this hypothesis by developing a network structure that matched the observed mTOR pathway dynamics, performing simulations, and then experimentally verifying the predictions. Consistent with this model, experimental testing showed that mTORC2 activity was sensitive to different modes of PI3K inhibition but was insensitive to constitutive activation of Akt in several cell types.

Dynamic modeling has been used extensively in the study of cell signaling networks, yielding many important insights related to cellular behavior (*75*). Here, we use dynamic modeling to discriminate among alternative network structures, in particular alternative modes of mTORC2 regulation. Others have used similar approaches to study the possible network structures for the segment polarity gene network (*76*) and the extracellular signal–regulated kinase pathway (*77*). Although network testing can be performed with a Bayesian statistical approach (*77*), we chose to perform experimental testing to distinguish among the proposed network topologies because our simulated conditions and outputs were experimentally tractable.

Because our approach relied on the simulation and experimental testing of differential network dynamics under the assumption of alternative network structures, this may have enabled us to identify a network structure for insulin-regulated mTORC2 activation that is different from any other regulatory mechanism proposed thus far. Our approach enabled exploration of the network dynamics of endogenous proteins, whereas other purely experimental studies have relied on approaches that interfere with the dynamics under investigation, for example, overexpression of mutagenized network components that uncouple upstream cues from feedback inhibition (*31*, *33*). We also confirmed mTOR-pS^{2481} as a specific and direct readout for mTORC2 activity, which unlike other mTORC2 readouts does not require activation by the NFL-dependent PI3K. Because we used changes in network dynamics as a means of testing alternative network structures and we used the phosphorylation status of mTOR Ser^{2481} as the readout of mTORC2 activity, this work is distinguishable from earlier studies (*31*, *33*, *35*), and these differences in the approach may account for the conclusion that mTORC2's induction is independent of TSC1-TSC2 and the NFL.

In addition to revealing a new mechanism of regulation of mTORC2 in response to insulin, our analyses revealed additional complexity in the regulation of Akt. Model parameterization revealed more complex dynamics for mTORC2s target site Ser^{473} in the AGC kinase Akt than for Ser^{2481} in mTOR, and this could not be explained exclusively by mTORC2 activation. To integrate Akt-pS^{473} dynamics into the dynamic network model, we had to estimate a second PDK2 that accounted for the early peak of Akt-pS^{473} at 3 min after induction with aa/insulin (Fig. 2A). In addition to mTORC2, various other PDK2 candidates for Akt have been reported, including DNA-PK (*78*, *79*), ILK (*80*), ATM (*81*), MAPKAPK-2 (*82*), PKC (*83*, *84*), Pak1 (*85*), and even Akt autophosphorylation (*86*), any of which may contribute to Akt-pS^{473} dynamics under different metabolic conditions. Furthermore, we observed that upon network perturbations involving the NFL, the dynamics of mTOR-pS^{2481} were different from those of Akt-pS^{473}, with only the latter resembling the PDK1 phosphorylation on Thr^{308} of Akt (Figs. 6A and 7A). Thus, the AGC kinase targets of mTORC2 were not suitable readouts of mTORC2 activity and could not be used in our system to analyze the dependence of mTORC2 activity on TSC1-TSC2 because TSC1-TSC2 inhibition induces NFL that inhibits PI3K, which in turn can affect AGC kinase phosphorylation by their PDK2s, independently of the actual PDK2 activity. Because of this complexity in Akt phosphorylation dynamics, we chose mTOR-pS^{2481} as the readout of mTORC2 activity. Although mTOR-pS^{2481} has been identified on Raptor-associated mTOR (mTORC1) and is rapamycin-sensitive in 3T3-L1 adipocytes (*62*, *64*), rapamycin did not affect mTOR-pS^{2481} in whole-cell lysates of human embryonic kidney (HEK) 293 cells (*64*) or Tag Jurkat cells (*61*). Soliman *et al.* (*64*) concluded that the rapamycin-insensitive, mTORC2-associated mTOR-pS^{2481} signal predominated over the rapamycin-sensitive, mTORC1-associated mTOR-pS^{2481} signal in HEK293 cells, possibly due to a relatively low abundance of mTORC1 compared to mTORC2. We also found that mTOR-pS^{2481} was predominantly associated with mTORC2 in HeLa cells, which we used for our experimental testing.

Our model assumes that the NFL is exclusively executed by p70-S6K, phosphorylating and thereby inhibiting IRS. GRB10-dependent IR inhibition in response to activated mTORC1 may also contribute to the NFL (*87*, *88*), thus adding more complexity to the NFL mechanism. Although the identification of GRB10 as a contributor to the NFL is mechanistically relevant, the effect is the same, namely, the inhibition of IRS in response to mTORC1 activity, and is readily detected by the reduction of Akt-pT^{308} upon high mTORC1 activity. Given the need to reduce the complexity of our model to enable parameterization, we did not introduce these mechanisms separately into our model, but combined them into one step.

Our data suggested that mTORC2 activity is independent of the NFL, which is consistent with previous studies (*31*, *33*). To ensure that we achieved full activation of both mTOR complexes and thus activation of the NFL, we stimulated the cells with both amino acids and insulin induction. We experimentally observed the activation of the NFL starting 45 min after induction, as measured by IRS1-pS^{636} (Fig. 2, A and B). Thus, under conditions in which the NFL was active, network perturbations inducing or inactivating the NFL did not affect mTORC2 activity as measured by mTOR-pS^{2481}.

Although mTORC2 activity was independent of the NFL, it was dependent on PI3K activity (Fig. 8, A and B). The dynamics of mTOR-pS^{2481} were not affected by inhibition of the TSC1-TSC2 complex or mTORC1, but were inhibited by pharmacological inhibition of PI3K or reduction in its downstream signaling by overexpression of PTEN. Because pharmacological inhibitors can have off-target effects, we used a maximum wortmannin concentration of 100 nM, which has been reported to specifically inhibit only class I PI3Ks (*72*). Although we found that mTOR-pS^{2481} dynamics were less sensitive to wortmannin than were the dynamics of the PDK1-targeted Akt-pT^{308}, mTOR-pS^{2481} inhibition occurred with wortmannin concentrations as low as 20 nM, indicating that mTORC2 inhibition was dependent on class I PI3K activity, which is consistent with previous studies (*61*, *64*). PDK1-deficient cells exhibited a wortmannin-sensitive phosphorylation on Ser^{473} of Akt (*89*), which, although not previously linked to mTORC2 activity, supports our hypothesis of a PI3K-dependent but Akt-independent (and therefore NFL- and TSC1-TSC2–independent) mTORC2 induction. This proposed PI3K regulatory

mechanism was surprising because PI3K induction by insulin is generally thought to be IRS-dependent (*1*), and IRS is inhibited by active p70-S6K and thereby mediates the NFL. Consequently, we propose that mTORC2 is induced by a PI3K species that is different from the PI3K that induces mTORC1, because mTORC1 activity strictly depends on TSC1-TSC2 and the NFL (*1*, *7*).

In our new proposed model for mTOR activation by insulin and amino acids, Akt should activate mTORC1 through the canonical insulin–IRS–PI3K–Akt–TSC1-TSC2 pathway, but should not participate in mTORC2 activation, which is induced by a different PI3K. Indeed, we showed in several cell lines that constitutively active Akt did not induce mTORC2 activity (mTOR-pS^{2481}), although it did activate mTORC1. Two studies have reported mTORC2 regulation downstream of PI3K that differs from the canonical Akt–TSC1-TSC2 signaling axis. Direct PI3K-dependent induction of mTORC2 by PtdIns(3,4,5)P_3 binding (*90*) has been observed, and ribosomal proteins have been described to bind and activate mTORC2 in a PI3K-dependent manner (*91*). Clearly, these mechanisms require further study, which will likely reveal further molecular connectors of PI3K and mTORC2.

What kind of mechanism could account for the observed NFL insensitivity of PI3K for mTORC2 induction? The NFL is mediated by IRS, which activates PI3K downstream of insulin and the IR (*1*). However, PI3K activity has also been observed in cells devoid of IRS protein (*92*, *93*), and the IR may activate PI3K in part by direct binding (*94*). Such IRS-independent PI3K activity might mediate NFL-independent stimulation of mTORC2 activity. For class I PI3Ks, there are at least seven alternative regulatory subunits and four alternative catalytic subunits, and specific combinations of these subunits might mediate different physiologic outputs. Receptor binding and abundance of the isoforms are differentially regulated by metabolic inputs, such as growth factors or amino acids (*95*). We may have detected this apparently IRS-independent PI3K activation because we used simultaneous stimulation with both insulin and amino acids to assure full induction of both mTOR complexes. In contrast, previous studies have mainly tested the effect of a single stimulus on class I PI3K activation. In a physiological environment, cells are confronted with multiple simultaneous inputs, and full activation of some PI3K isoforms can require multiple upstream inputs (*95*). Hence, the existence of an NFL-independent class I PI3K is conceivable and requires further investigation.

In conclusion, the suggested novel network structure, connecting mTORC2 to its upstream inputs, is supported by the existing literature and reveals a need to reevaluate the mTORC2 regulatory mechanisms. The complexity of differential mTORC1 and mTORC2 regulation that we propose highlights the need to apply integrated computational-experimental approaches to understand complex signaling and regulatory networks. Because our dynamic model of mTORC1 and mTORC2 signaling is a mathematical representation of the differential signal transduction toward mTORC1 and mTORC2, it enables simulation of the signaling dynamics that are transmitted through the network under different metabolic conditions. Moreover, despite being a simplification, our model simulations mathematically showed that the simplified system was sufficient to explain the experimental observations. The fully parameterized model provides a resource for future work and other modeling efforts can extend and build upon it, as well as provide a framework on which pharmacological interventions can be tested.

MATERIALS AND METHODS

Lentiviral knockdown cell lines

Experiments were performed in HeLa α Kyoto cells and C2C12 myoblasts. For inducible knockdown of Raptor or TSC2, cells were transduced with lentivirus encoding the tetracycline-sensitive tTR-KRAB repressor and a DsRed reporter (*96*). Cells were subsequently transfected with lentivirus encoding the specific short hairpin RNA (target sequence Raptor: 5′-GGCTAGTCTGTTTCGAAATTT-3′, TSC2: 5′-CGACGAGTCAAACAAGCCAAT-3′), and a green fluorescent protein (GFP) reporter (pLVTH vector), both under the control of tTR-KRAB. For lentivirus-mediated knockdown of Rictor, a pLKO.1-based short hairpin construct specific for Rictor (Addgene plasmid 1853) and a scrambled control sequence (Addgene plasmid 1864) were obtained from Addgene (*21*). HeLa cells were transfected with viral supernatant twice as described previously (*63*) and harvested 60 hours after transfection.

Overexpression of PTEN and myr-Akt variants

Plasmids were ordered from Addgene: N-terminally hemagglutinin (HA)–tagged pSG5L HA PTEN wild type, N-terminally myristoylated and HA-tagged pLNCX.myr.HA.Akt1, and N-terminally myristoylated and HA-tagged, kinase-dead pLNCX.myr.HA.Akt1 K179M. Transfection was performed with 6 μg per 6-cm dish by the use of JetPEI reagent according to the manufacturer's instructions. Cells were harvested 24 hours after transfection.

Antibodies and reagents

The antibody recognizing PRAS40 (Ser^{183} phosphorylated) was purchased from IBL. The polyclonal antibody recognizing PRAS40 (Thr^{246} phosphorylated) was purchased from Biosource. The monoclonal antibody recognizing glyceraldehyde-3-phosphate dehydrogenase (GAPDH) was purchased from Abcam. The antibody recognizing Rictor was purchased from Bethyl. Horseradish peroxidase (HRP)–conjugated goat anti-mouse and goat anti-rabbit immunoglobulin G (IgG) were purchased from Pierce Biotechnology (Thermo Scientific). Antibodies recognizing Akt, phospho-Akt (Thr^{308}), phospho-Akt (Ser^{473}), phospho–IGF-I receptor β (Tyr^{1131})/IRβ (Tyr^{1146}), IRS-1, phospho–IRS-1 (Ser$^{636/639}$), mTOR, phospho-mTOR (Ser^{2448}), phospho-mTOR (Ser^{2481}), PRAS40, p70S6K, phospho-p70S6K (Thr^{389}), and TSC2 were purchased from Cell Signaling Technology. The antibody recognizing IRβ was purchased from Santa Cruz Biotechnology. Rapamycin and LY294002 were purchased from Calbiochem, Merck. PP242 and wortmannin were purchased from Sigma-Aldrich. Chemicals were supplied by Carl Roth if not indicated otherwise.

Immunoprecipitation

Immunoprecipitations were performed as described elsewhere (*13*, *19*). Lysis buffer was complemented with protease inhibitors (Complete; Roche), Phosphatase Inhibitor Cocktail 2, Phosphatase Inhibitor Cocktail 3 (both Sigma-Aldrich), and PP242 to inhibit residual mTOR activity after the time of lysis. Immunoprecipitations were performed with antibody (5 μg/ml) [antibody recognizing Sin1, Raptor, or rabbit IgG (all Bethyl)] and with magnetic Dynabeads Protein G (Invitrogen).

Analysis of whole-cell lysates

For calibration data sets, HeLa cells were starved for serum and amino acids by exchanging standard growth medium for Hank's buffered salt solution (HBSS) (PAN Biotech GmbH) overnight to inhibit mTOR pathway activity. After 16 hours of starvation, mTOR signaling was restimulated with Dulbecco's modified Eagle's medium (DMEM) containing amino acids and supplemented with 100 nM insulin (Sigma-Aldrich).

Gradual knockdowns of Raptor or TSC2 were established by induction with doxycycline (5 μg/ml; Calbiochem, Merck) for 0, 1, 2, or 3 days. Cells were starved for 16 hours in HBSS and mTOR signaling was induced with DMEM (PAA) supplemented with 100 nM insulin. PP242 and rapamycin were added 1 hour before lysis. Wortmannin or LY294002 was

added 30 min before and during the stimulation with DMEM supplemented with 100 nM insulin. Cells were washed once with phosphate-buffered saline (PBS) and lysed with TNE lysis buffer [50 mM tris-HCl (pH 8.0), 150 mM NaCl, 1% (v/v) Triton X-100 (Calbiochem, Merck), Complete (Roche), Phosphatase Inhibitor Cocktail 2, and Phosphatase Inhibitor Cocktail 3 (both Sigma-Aldrich)]. Protein concentrations were measured (Protein Assay Dye Reagent Concentrate, Bio-Rad) according to the manufacturer's protocol. Concentrations were adjusted with lysis buffer. Lysates were diluted in sample buffer [5×: 6 ml glycerol, 0.6 ml β-mercaptoethanol, 1.0 g SDS, 3.75 ml 1 M tris (pH 6.8), 2 mg bromophenol blue, and 2 ml H_2O]. Whole-cell lysates were analyzed with SDS–polyacrylamide gel electrophoresis (SDS-PAGE) gels. Proteins were transferred to polyvinylidene difluoride (PVDF) membranes (Millipore), blocked with 5% bovine serum albumin (BSA) in TBST [8 g NaCl, 0.2 g KCl, 8 g tris (pH 7.4), 0.1% Tween 20] for a minimum of 30 min, and incubated with the primary antibody in 5% BSA in TBST overnight with shaking at 4°C. Blots were washed three times with TBST, incubated with secondary antibodies coupled to HRP, and washed three times with TBST before detection.

Quantitation of immunoblots

HRP was detected with the ECL Western Blotting Substrate or the SuperSignal West Femto reagent (Pierce Biotechnology, Thermo Scientific), and the emitted light was detected and quantified with a chemiluminescence imaging analyzer (LAS 4000 mini; Fujifilm). Obtained images were analyzed with Multi-Gauge version 3.0 software (Fujifilm). Local background was subtracted. All data were normalized against GAPDH. Representative blots were exported as TIF files and processed with Adobe Photoshop.

Modeling

CellDesigner 4.2 (*97*) was used to construct the model network topology in SBGN (*59*). COPASI 4.7.34 (*98*) was used for all deterministic simulations, parameter estimations, parameter scanning, and sensitivity analysis. The deterministic simulation algorithm (LSODA) was configured with the following parameters: duration, 1440; interval size, 1; intervals, 1440; integrate reduced model, 0; relative tolerance, 1×10^{-6}; absolute tolerance, 1×10^{-12}; maximum internal steps, 10,000. The algorithm used for parameter estimation was simulated annealing (*99*, *100*), configured with the following parameters: start temperature, 1; cooling factor, 0.85; tolerance, 1×10^{-6}; random number generator, 1; seed, 0. The parameter estimation weight method was mean square and the experiment type was time course. The initial concentration of the species in nonphosphorylated state was fixed to the maximum intensity of the third quantile time course, computed from the four experimental data sets, of the corresponding experimental phosphorylated protein. This ensured that the modeled kinases did not saturate their substrates and that the concentrations of the substrates remained small. The initial concentration of the species in any other state was fixed to 0. The initial concentration of PDK2 was assumed to be equal to the concentration of the β subunit of the IR because the two species are directly connected in the model. In the absence of experimental data for the TSC complex, the initial concentration was assumed to be 10. The models were formalized with only mass action reactions. For each phase, the kinetic rate constants were estimated by running 350 independent calibrations, each initialized with a random initial configuration of the parameters. The parameter values were constrained within the interval $[1 \times 10^{-4}, 1]$ except for the Akt parameters, which were constrained within the interval $[1 \times 10^{-4}, 10]$. For each calibration phase (F), the solutions of the estimations consistent with the data and achieving the lowest root mean square error (RMSE) were selected as the best solutions set (BS). Among these, the solution closest to the centroid of the BS cluster in the parameter space was selected with the following formula:

$$\arg\min_{S \in \mathrm{BS_F}} \sum_{i=1}^{N} (S(p_i) - \mu_i)^2$$

where $\mathrm{BS_F} = \{x | \forall\, y \in \mathrm{AllSolutions}, \mathrm{RMSE}(\mathrm{Model}(x), \mathrm{Data}) \leq \mathrm{RMSE}(\mathrm{Model}(y), \mathrm{Data})\}$, p_i is the ith estimated parameter in S, μ_i is the ith parameter mean computed from $\mathrm{BS_F}$, and N is the number of estimated parameters.

Model identifiability based on correlation analysis of sensitivity trajectories was calculated with SBToolbox2 and SBPDToolbox (*101*) for MATLAB. SBMLToolbox 4.0.1 (*102*) was used to import our SBML models into SBToolbox2. Identifiability analysis tables for the general model and the four hypotheses models are depicted in figs. S5, S8, S10, S12, and S17.

All parameter values for the final models are given in tables S2 and S3. The sensitivity analysis algorithm was configured for time series with the following parameters: Delta factor, 0.001, and Delta minimum, 1×10^{-12} (figs. S6, S9, S11, S13, and S18). We also used COPASI and CellDesigner to export the models as SBML (*103*) Level 2 Version 4 (models S1 to S5). CellDesigner was used to generate the extended mTOR network model in SBGN (*59*) graphical notation (model S6).

Statistics

The statistical and programming language R version 2.12.1 (*104*) was used to calculate the statistics and generate the plots. The SEM was chosen to estimate the statistical variability of the measured samples of experimental time course. Model goodness of fit was defined by computing Akaike information criterion (*105*) and χ^2 was calculated as follows:

$$\chi^2 = \sum_{i=1}^{N} \left(\frac{y_i - \mu(d_i)}{\sigma(d_i)} \right)^2$$

where N is the number of experimental data points and $y_i - \mu(d_i)$ is the ith residual between the simulated and the experimental mean data point, which is normalized by the SD of the same data point. For the general model and the four hypotheses, χ^2 and Akaike information criterion measures are provided in table S4. Tukey's honest significant differences (HSD) test, in conjunction with one-way analysis of variance (ANOVA), was used as statistical test for multiple comparisons among groups of experimental data.

SUPPLEMENTARY MATERIALS

www.sciencesignaling.org/cgi/content/full/5/217/ra25/DC1

Fig. S1. Extended graphical model of the mammalian TOR network.
Fig. S2. A linear relationship between Western blot signals and protein concentrations.
Fig. S3. Phases of the calibration process.
Fig. S4. Details of a calibration phase.
Fig. S5. Identifiability analysis for the general model.
Fig. S6. Sensitivity analysis for the general model.
Fig. S7. Comparison between the simulated and experimental time courses for hypotheses 1, 2, and 3 for readouts of the mTOR network.
Fig. S8. Identifiability analysis for hypothesis 1: TSC1-TSC2–dependent hypothesis mTORC2 regulation.
Fig. S9. Sensitivity analysis for hypothesis 1: TSC1-TSC2–dependent hypothesis mTORC2 regulation.
Fig. S10. Identifiability analysis for hypothesis 2: NFL-mTORC2 regulation.
Fig. S11. Sensitivity analysis for hypothesis 2: NFL-mTORC2 regulation.
Fig. S12. Identifiability analysis for hypothesis 3: PI3K-independent mTORC2 regulation.

Fig. S13. Sensitivity analysis for hypothesis 3: PI3K-independent mTORC2 regulation.
Fig. S14. The influence of perturbations of TSC1-TSC2, mTORC1, and PI3K on the phosphorylation of Akt-T^{308} for the three hypotheses.
Fig. S15. The influence of perturbations of TSC1-TSC2, mTORC1, and PI3K on the phosphorylation of p70-S6K-T^{389} for the three hypotheses.
Fig. S16. Simulation and perturbations for the new network structure based on hypothesis 4: PI3K-dependent, NFL-independent regulation of mTORC2.
Fig. S17. Identifiability analysis for hypothesis 4: PI3K-dependent, NFL-independent regulation of mTORC2.
Fig. S18. Sensitivity analysis for hypothesis 4: PI3K-dependent, NFL-independent regulation of mTORC2.
Table S1. Ordinary differential equations of the general model and the models representing hypotheses, 1, 2, and 3 for mTORC2 activation.
Table S2. Parameter values of the general model.
Table S3. Parameter values of hypotheses 1, 2, and 3.
Table S4. Summary of model goodness of fit.
Models S1 to S6.

REFERENCES AND NOTES

1. R. Zoncu, A. Efeyan, D. M. Sabatini, mTOR: From growth signal integration to cancer, diabetes and ageing. *Nat. Rev. Mol. Cell Biol.* **12**, 21–35 (2011).
2. J. J. Howell, B. D. Manning, mTOR couples cellular nutrient sensing to organismal metabolic homeostasis. *Trends Endocrinol. Metab.* **22**, 94–102 (2011).
3. C. Garcia-Echeverria, Blocking the mTOR pathway: A drug discovery perspective. *Biochem. Soc. Trans.* **39**, 451–455 (2011).
4. P. Polak, M. N. Hall, mTOR and the control of whole body metabolism. *Curr. Opin. Cell Biol.* **21**, 209–218 (2009).
5. N. Cybulski, M. N. Hall, TOR complex 2: A signaling pathway of its own. *Trends Biochem. Sci.* **34**, 620–627 (2009).
6. M. E. Feldman, K. M. Shokat, New inhibitors of the PI3K-Akt-mTOR pathway: Insights into mTOR signaling from a new generation of Tor kinase domain inhibitors (TORKinibs). *Curr. Top. Microbiol. Immunol.* **347**, 241–262 (2010).
7. S. Sengupta, T. R. Peterson, D. M. Sabatini, Regulation of the mTOR complex 1 pathway by nutrients, growth factors, and stress. *Mol. Cell* **40**, 310–322 (2010).
8. Y. Sancak, L. Bar-Peled, R. Zoncu, A. L. Markhard, S. Nada, D. M. Sabatini, Ragulator-Rag complex targets mTORC1 to the lysosomal surface and is necessary for its activation by amino acids. *Cell* **141**, 290–303 (2010).
9. Y. Sancak, D. M. Sabatini, Rag proteins regulate amino-acid-induced mTORC1 signalling. *Biochem. Soc. Trans.* **37**, 289–290 (2009).
10. J. Avruch, X. Long, Y. Lin, S. Ortiz-Vega, J. Rapley, A. Papageorgiou, N. Oshiro, U. Kikkawa, Activation of mTORC1 in two steps: Rheb-GTP activation of catalytic function and increased binding of substrates to raptor. *Biochem. Soc. Trans.* **37**, 223–226 (2009).
11. K. Thedieck, M. N. Hall, in *The Handbook of Cell Signaling*, R. Bradshaw, E. Dennis, Eds. (Elsevier, San Diego, CA, 2009), vol. 3, chap. 274, pp. 2285–2293.
12. E. Vander Haar, S. I. Lee, S. Bandhakavi, T. J. Griffin, D. H. Kim, Insulin signalling to mTOR mediated by the Akt/PKB substrate PRAS40. *Nat. Cell Biol.* **9**, 316–323 (2007).
13. K. Thedieck, P. Polak, M. L. Kim, K. D. Molle, A. Cohen, P. Jenö, C. Arrieumerlou, M. N. Hall, PRAS40 and PRR5-like protein are new mTOR interactors that regulate apoptosis. *PLoS One* **2**, e1217 (2007).
14. Y. Sancak, C. C. Thoreen, T. R. Peterson, R. A. Lindquist, S. A. Kang, E. Spooner, S. A. Carr, D. M. Sabatini, PRAS40 is an insulin-regulated inhibitor of the mTORC1 protein kinase. *Mol. Cell* **25**, 903–915 (2007).
15. L. Wang, T. E. Harris, R. A. Roth, J. C. Lawrence Jr., PRAS40 regulates mTORC1 kinase activity by functioning as a direct inhibitor of substrate binding. *J. Biol. Chem.* **282**, 20036–20044 (2007).
16. B. D. Fonseca, E. M. Smith, V. H. Lee, C. MacKintosh, C. G. Proud, PRAS40 is a target for mammalian target of rapamycin complex 1 and is required for signaling downstream of this complex. *J. Biol. Chem.* **282**, 24514–24524 (2007).
17. N. Oshiro, R. Takahashi, K. Yoshino, K. Tanimura, A. Nakashima, S. Eguchi, T. Miyamoto, K. Hara, K. Takehana, J. Avruch, U. Kikkawa, K. Yonezawa, The proline-rich Akt substrate of 40 kDa (PRAS40) is a physiological substrate of mammalian target of rapamycin complex 1. *J. Biol. Chem.* **282**, 20329–20339 (2007).
18. L. Wang, T. E. Harris, J. C. Lawrence Jr., Regulation of proline-rich Akt substrate of 40 kDa (PRAS40) function by mammalian target of rapamycin complex 1 (mTORC1)-mediated phosphorylation. *J. Biol. Chem.* **283**, 15619–15627 (2008).
19. E. Jacinto, R. Loewith, A. Schmidt, S. Lin, M. A. Ruegg, A. Hall, M. N. Hall, Mammalian TOR complex 2 controls the actin cytoskeleton and is rapamycin insensitive. *Nat. Cell Biol.* **6**, 1122–1128 (2004).
20. I. Tato, R. Bartrons, F. Ventura, J. L. Rosa, Amino acids activate mammalian target of rapamycin complex 2 (mTORC2) via PI3K/Akt signaling. *J. Biol. Chem.* **286**, 6128–6142 (2011).
21. D. D. Sarbassov, D. A. Guertin, S. M. Ali, D. M. Sabatini, Phosphorylation and regulation of Akt/PKB by the rictor-mTOR complex. *Science* **307**, 1098–1101 (2005).
22. E. Jacinto, V. Facchinetti, D. Liu, N. Soto, S. Wei, S. Y. Jung, Q. Huang, J. Qin, B. Su, SIN1/MIP1 maintains rictor-mTOR complex integrity and regulates Akt phosphorylation and substrate specificity. *Cell* **127**, 125–137 (2006).
23. C. Shiota, J. T. Woo, J. Lindner, K. D. Shelton, M. A. Magnuson, Multiallelic disruption of the *rictor* gene in mice reveals that mTOR complex 2 is essential for fetal growth and viability. *Dev. Cell* **11**, 583–589 (2006).
24. R. C. Hresko, M. Mueckler, mTOR·RICTOR is the Ser^{473} kinase for Akt/protein kinase B in 3T3-L1 adipocytes. *J. Biol. Chem.* **280**, 40406–40416 (2005).
25. J. M. García-Martínez, D. R. Alessi, mTOR complex 2 (mTORC2) controls hydrophobic motif phosphorylation and activation of serum- and glucocorticoid-induced protein kinase 1 (SGK1). *Biochem. J.* **416**, 375–385 (2008).
26. D. D. Sarbassov, S. M. Ali, D. H. Kim, D. A. Guertin, R. R. Latek, H. Erdjument-Bromage, P. Tempst, D. M. Sabatini, Rictor, a novel binding partner of mTOR, defines a rapamycin-insensitive and raptor-independent pathway that regulates the cytoskeleton. *Curr. Biol.* **14**, 1296–1302 (2004).
27. L. R. Pearce, D. Komander, D. R. Alessi, The nuts and bolts of AGC protein kinases. *Nat. Rev. Mol. Cell Biol.* **11**, 9–22 (2010).
28. E. Jacinto, A. Lorberg, TOR regulation of AGC kinases in yeast and mammals. *Biochem. J.* **410**, 19–37 (2008).
29. E. Fayard, G. Xue, A. Parcellier, L. Bozulic, B. A. Hemmings, Protein kinase B (PKB/Akt), a key mediator of the PI3K signaling pathway. *Curr. Top. Microbiol. Immunol.* **346**, 31–56 (2010).
30. K. Inoki, M. N. Corradetti, K. L. Guan, Dysregulation of the TSC-mTOR pathway in human disease. *Nat. Genet.* **37**, 19–24 (2005).
31. J. Huang, C. C. Dibble, M. Matsuzaki, B. D. Manning, The TSC1-TSC2 complex is required for proper activation of mTOR complex 2. *Mol. Cell. Biol.* **28**, 4104–4115 (2008).
32. J. Huang, B. D. Manning, A complex interplay between Akt, TSC2 and the two mTOR complexes. *Biochem. Soc. Trans.* **37**, 217–222 (2009).
33. J. Huang, S. Wu, C. L. Wu, B. D. Manning, Signaling events downstream of mammalian target of rapamycin complex 2 are attenuated in cells and tumors deficient for the tuberous sclerosis complex tumor suppressors. *Cancer Res.* **69**, 6107–6114 (2009).
34. W. van Veelen, S. E. Korsse, L. van de Laar, M. P. Peppelenbosch, The long and winding road to rational treatment of cancer associated with LKB1/AMPK/TSC/mTORC1 signaling. *Oncogene* **30**, 2289–2303 (2011).
35. Q. Yang, K. Inoki, E. Kim, K. L. Guan, TSC1/TSC2 and Rheb have different effects on TORC1 and TORC2 activity. *Proc. Natl. Acad. Sci. U.S.A.* **103**, 6811–6816 (2006).
36. E. A. Goncharova, D. A. Goncharov, H. Li, W. Pimtong, S. Lu, I. Khavin, V. P. Krymskaya, mTORC2 is required for proliferation and survival of TSC2-null cells. *Mol. Cell. Biol.* **31**, 2484–2498 (2011).
37. Y. Kamimura, Y. Xiong, P. A. Iglesias, O. Hoeller, P. Bolourani, P. N. Devreotes, PIP_3-independent activation of TorC2 and PKB at the cell's leading edge mediates chemotaxis. *Curr. Biol.* **18**, 1034–1043 (2008).
38. S. Lee, Z. Shen, D. N. Robinson, S. Briggs, R. A. Firtel, Involvement of the cytoskeleton in controlling leading-edge function during chemotaxis. *Mol. Biol. Cell* **21**, 1810–1824 (2010).
39. P. G. Charest, Z. Shen, A. Lakoduk, A. T. Sasaki, S. P. Briggs, R. A. Firtel, A Ras signaling complex controls the RasC-TORC2 pathway and directed cell migration. *Dev. Cell* **18**, 737–749 (2010).
40. H. Cai, S. Das, Y. Kamimura, Y. Long, C. A. Parent, P. N. Devreotes, Ras-mediated activation of the TORC2–PKB pathway is critical for chemotaxis. *J. Cell Biol.* **190**, 233–245 (2010).
41. G. S. Worthen, N. Avdi, A. M. Buhl, N. Suzuki, G. L. Johnson, FMLP activates Ras and Raf in human neutrophils. Potential role in activation of MAP kinase. *J. Clin. Invest.* **94**, 815–823 (1994).
42. L. Zheng, J. Eckerdal, I. Dimitrijevic, T. Andersson, Chemotactic peptide-induced activation of Ras in human neutrophils is associated with inhibition of p120-GAP activity. *J. Biol. Chem.* **272**, 23448–23454 (1997).
43. Y. Kamada, Y. Fujioka, N. N. Suzuki, F. Inagaki, S. Wullschleger, R. Loewith, M. N. Hall, Y. Ohsumi, Tor2 directly phosphorylates the AGC kinase Ypk2 to regulate actin polarization. *Mol. Cell. Biol.* **25**, 7239–7248 (2005).
44. E. Caron, S. Ghosh, Y. Matsuoka, D. Ashton-Beaucage, M. Therrien, S. Lemieux, C. Perreault, P. P. Roux, H. Kitano, A comprehensive map of the mTOR signaling network. *Mol. Syst. Biol.* **6**, 453 (2010).
45. P. Jain, U. S. Bhalla, Signaling logic of activity-triggered dendritic protein synthesis: An mTOR gate but not a feedback switch. *PLoS Comput. Biol.* **5**, e1000287 (2009).
46. C. Brännmark, R. Palmér, S. T. Glad, G. Cedersund, P. Strålfors, Mass and information feedbacks through receptor endocytosis govern insulin signaling as revealed using a parameter-free modeling framework. *J. Biol. Chem.* **285**, 20171–20179 (2010).
47. D. Ruths, M. Muller, J. T. Tseng, L. Nakhleh, P. T. Ram, The signaling Petri net-based simulator: A non-parametric strategy for characterizing the dynamics of cell-specific signaling networks. *PLoS Comput. Biol.* **4**, e1000005 (2008).

48. N. Borisov, E. Aksamitiene, A. Kiyatkin, S. Legewie, J. Berkhout, T. Maiwald, N. P. Kaimachnikov, J. Timmer, J. B. Hoek, B. N. Kholodenko, Systems-level interactions between insulin-EGF networks amplify mitogenic signaling. *Mol. Syst. Biol.* **5**, 256 (2009).
49. G. Cedersund, J. Roll, E. Ulfhielm, A. Danielsson, H. Tidefelt, P. Strålfors, Model-based hypothesis testing of key mechanisms in initial phase of insulin signaling. *PLoS Comput. Biol.* **4**, e1000096 (2008).
50. V. V. Kiselyov, S. Versteyhe, L. Gauguin, P. De Meyts, Harmonic oscillator model of the insulin and IGF1 receptors' allosteric binding and activation. *Mol. Syst. Biol.* **5**, 243 (2009).
51. D. Faratian, A. Goltsov, G. Lebedeva, A. Sorokin, S. Moodie, P. Mullen, C. Kay, I. H. Um, S. Langdon, I. Goryanin, D. J. Harrison, Systems biology reveals new strategies for personalizing cancer medicine and confirms the role of PTEN in resistance to trastuzumab. *Cancer Res.* **69**, 6713–6720 (2009).
52. L. Kuepfer, M. Peter, U. Sauer, J. Stelling, Ensemble modeling for analysis of cell signaling dynamics. *Nat. Biotechnol.* **25**, 1001–1006 (2007).
53. S. Nelander, W. Wang, B. Nilsson, Q. B. She, C. Pratilas, N. Rosen, P. Gennemark, C. Sander, Models from experiments: Combinatorial drug perturbations of cancer cells. *Mol. Syst. Biol.* **4**, 216 (2008).
54. A. R. Sedaghat, A. Sherman, M. J. Quon, A mathematical model of metabolic insulin signaling pathways. *Am. J. Physiol. Endocrinol. Metab.* **283**, E1084–E1101 (2002).
55. G. Wang, G. R. Krueger, Computational analysis of mTOR signaling pathway: Bifurcation, carcinogenesis, and drug discovery. *Anticancer Res.* **30**, 2683–2688 (2010).
56. P. K. Vinod, K. V. Venkatesh, Quantification of the effect of amino acids on an integrated mTOR and insulin signaling pathway. *Mol. Biosyst.* **5**, 1163–1173 (2009).
57. G. R. Smith, D. P. Shanley, Modelling the response of FOXO transcription factors to multiple post-translational modifications made by ageing-related signalling pathways. *PLoS One* **5**, e11092 (2010).
58. J. A. Papin, T. Hunter, B. O. Palsson, S. Subramaniam, Reconstruction of cellular signalling networks and analysis of their properties. *Nat. Rev. Mol. Cell Biol.* **6**, 99–111 (2005).
59. N. Le Novere, M. Hucka, H. Mi, S. Moodie, F. Schreiber, A. Sorokin, E. Demir, K. Wegner, M. I. Aladjem, S. M. Wimalaratne, F. T. Bergman, R. Gauges, P. Ghazal, H. Kawaji, L. Li, Y. Matsuoka, A. Villeger, S. E. Boyd, L. Calzone, M. Courtot, U. Dogrusoz, T. C. Freeman, A. Funahashi, S. Ghosh, A. Jouraku, S. Kim, F. Kolpakov, A. Luna, S. Sahle, E. Schmidt, S. Watterson, G. Wu, I. Goryanin, D. B. Kell, C. Sander, H. Sauro, J. L. Snoep, K. Kohn, H. Kitano, The Systems Biology Graphical Notation. *Nat. Biotechnol.* **27**, 735–741 (2009).
60. M. A. Bruhn, R. B. Pearson, R. D. Hannan, K. E. Sheppard, Second AKT: The rise of SGK in cancer signalling. *Growth Factors* **28**, 394–408 (2010).
61. R. T. Peterson, P. A. Beal, M. J. Comb, S. L. Schreiber, FKBP12-rapamycin-associated protein (FRAP) autophosphorylates at serine 2481 under translationally repressive conditions. *J. Biol. Chem.* **275**, 7416–7423 (2000).
62. H. A. Acosta-Jaquez, J. A. Keller, K. G. Foster, B. Ekim, G. A. Soliman, E. P. Feener, B. A. Ballif, D. C. Fingar, Site-specific mTOR phosphorylation promotes mTORC1-mediated signaling and cell growth. *Mol. Cell. Biol.* **29**, 4308–4324 (2009).
63. J. Copp, G. Manning, T. Hunter, TORC-specific phosphorylation of mammalian target of rapamycin (mTOR): Phospho-Ser^{2481} is a marker for intact mTOR signaling complex 2. *Cancer Res.* **69**, 1821–1827 (2009).
64. G. A. Soliman, H. A. Acosta-Jaquez, E. A. Dunlop, B. Ekim, N. E. Maj, A. R. Tee, D. C. Fingar, mTOR Ser-2481 autophosphorylation monitors mTORC-specific catalytic activity and clarifies rapamycin mechanism of action. *J. Biol. Chem.* **285**, 7866–7879 (2010).
65. M. E. Feldman, B. Apsel, A. Uotila, R. Loewith, Z. A. Knight, D. Ruggero, K. M. Shokat, Active-site inhibitors of mTOR target rapamycin-resistant outputs of mTORC1 and mTORC2. *PLoS Biol.* **7**, e38 (2009).
66. C. C. Thoreen, S. A. Kang, J. W. Chang, Q. Liu, J. Zhang, Y. Gao, L. J. Reichling, T. Sim, D. M. Sabatini, N. S. Gray, An ATP-competitive mammalian target of rapamycin inhibitor reveals rapamycin-resistant functions of mTORC1. *J. Biol. Chem.* **284**, 8023–8032 (2009).
67. C. C. Thoreen, D. M. Sabatini, Rapamycin inhibits mTORC1, but not completely. *Autophagy* **5**, 725–726 (2009).
68. F. Heidebrecht, A. Heidebrecht, I. Schulz, S. E. Behrens, A. Bader, Improved semi-quantitative Western blot technique with increased quantification range. *J. Immunol. Methods* **345**, 40–48 (2009).
69. W. W. Chen, M. Niepel, P. K. Sorger, Classic and contemporary approaches to modeling biochemical reactions. *Genes Dev.* **24**, 1861–1875 (2010).
70. C. G. Moles, P. Mendes, J. R. Banga, Parameter estimation in biochemical pathways: A comparison of global optimization methods. *Genome Res.* **13**, 2467–2474 (2003).
71. C. Zhan, L. F. Yeung, Parameter estimation in systems biology models using spline approximation. *BMC Syst. Biol.* **5**, 14 (2011).
72. G. J. Brunn, J. Williams, C. Sabers, G. Wiederrecht, J. C. Lawrence Jr., R. T. Abraham, Direct inhibition of the signaling functions of the mammalian target of rapamycin by the phosphoinositide 3-kinase inhibitors, wortmannin and LY294002. *EMBO J.* **15**, 5256–5267 (1996).
73. R. D. Polakiewicz, S. M. Schieferl, A. C. Gingras, N. Sonenberg, M. J. Comb, μ-Opioid receptor activates signaling pathways implicated in cell survival and translational control. *J. Biol. Chem.* **273**, 23534–23541 (1998).
74. A. D. Kohn, F. Takeuchi, R. A. Roth, Akt, a pleckstrin homology domain containing kinase, is activated primarily by phosphorylation. *J. Biol. Chem.* **271**, 21920–21926 (1996).
75. B. N. Kholodenko, Cell-signalling dynamics in time and space. *Nat. Rev. Mol. Cell Biol.* **7**, 165–176 (2006).
76. G. von Dassow, E. Meir, E. M. Munro, G. M. Odell, The segment polarity network is a robust developmental module. *Nature* **406**, 188–192 (2000).
77. T.-R. Xu, V. Vyshemirsky, A. Gormand, A. von Kriegsheim, M. Girolami, G. S. Baillie, D. Ketley, A. J. Dunlop, G. Milligan, M. D. Houslay, W. Kolch, Inferring signaling pathway topologies from multiple perturbation measurements of specific biochemical species. *Sci. Signal.* **3**, ra20 (2010).
78. L. Bozulic, B. Surucu, D. Hynx, B. A. Hemmings, PKBα/Akt1 acts downstream of DNA-PK in the DNA double-strand break response and promotes survival. *Mol. Cell* **30**, 203–213 (2008).
79. J. Feng, J. Park, P. Cron, D. Hess, B. A. Hemmings, Identification of a PKB/Akt hydrophobic motif Ser-473 kinase as DNA-dependent protein kinase. *J. Biol. Chem.* **279**, 41189–41196 (2004).
80. A. A. Troussard, N. M. Mawji, C. Ong, A. Mui, R. St-Arnaud, S. Dedhar, Conditional knock-out of integrin-linked kinase demonstrates an essential role in protein kinase B/Akt activation. *J. Biol. Chem.* **278**, 22374–22378 (2003).
81. J. G. Viniegra, N. Martinez, P. Modirassari, J. H. Losa, C. Parada Cobo, V. J. Lobo, C. I. Luquero, L. Alvarez-Vallina, S. Ramón y Cajal, J. M. Rojas, R. Sánchez-Prieto, Full activation of PKB/Akt in response to insulin or ionizing radiation is mediated through ATM. *J. Biol. Chem.* **280**, 4029–4036 (2005).
82. M. J. Rane, P. Y. Coxon, D. W. Powell, R. Webster, J. B. Klein, W. Pierce, P. Ping, K. R. McLeish, p38 kinase-dependent MAPKAPK-2 activation functions as 3-phosphoinositide-dependent kinase-2 for Akt in human neutrophils. *J. Biol. Chem.* **276**, 3517–3523 (2001).
83. Y. Kawakami, H. Nishimoto, J. Kitaura, M. Maeda-Yamamoto, R. M. Kato, D. R. Littman, M. Leitges, D. J. Rawlings, T. Kawakami, Protein kinase C βII regulates Akt phosphorylation on Ser-473 in a cell type- and stimulus-specific fashion. *J. Biol. Chem.* **279**, 47720–47725 (2004).
84. C. Partovian, M. Simons, Regulation of protein kinase B/Akt activity and Ser^{473} phosphorylation by protein kinase Cα in endothelial cells. *Cell. Signal.* **16**, 951–957 (2004).
85. K. Mao, S. Kobayashi, Z. M. Jaffer, Y. Huang, P. Volden, J. Chernoff, Q. Liang, Regulation of Akt/PKB activity by P21-activated kinase in cardiomyocytes. *J. Mol. Cell. Cardiol.* **44**, 429–434 (2008).
86. A. Toker, A. C. Newton, Akt/protein kinase B is regulated by autophosphorylation at the hypothetical PDK-2 site. *J. Biol. Chem.* **275**, 8271–8274 (2000).
87. Y. Yu, S. O. Yoon, G. Poulogiannis, Q. Yang, X. M. Ma, J. Villén, N. Kubica, G. R. Hoffman, L. C. Cantley, S. P. Gygi, J. Blenis, Phosphoproteomic analysis identifies Grb10 as an mTORC1 substrate that negatively regulates insulin signaling. *Science* **332**, 1322–1326 (2011).
88. P. P. Hsu, S. A. Kang, J. Rameseder, Y. Zhang, K. A. Ottina, D. Lim, T. R. Peterson, Y. Choi, N. S. Gray, M. B. Yaffe, J. A. Marto, D. M. Sabatini, The mTOR-regulated phosphoproteome reveals a mechanism of mTORC1-mediated inhibition of growth factor signaling. *Science* **332**, 1317–1322 (2011).
89. M. R. Williams, J. S. Arthur, A. Balendran, J. van der Kaay, V. Poli, P. Cohen, D. R. Alessi, The role of 3-phosphoinositide-dependent protein kinase 1 in activating AGC kinases defined in embryonic stem cells. *Curr. Biol.* **10**, 439–448 (2000).
90. X. Gan, J. Wang, B. Su, D. Wu, Evidence for direct activation of mTORC2 kinase activity by phosphatidylinositol 3,4,5-trisphosphate. *J. Biol. Chem.* **286**, 10998–11002 (2011).
91. V. Zinzalla, D. Stracka, W. Oppliger, M. N. Hall, Activation of mTORC2 by association with the ribosome. *Cell* **144**, 757–768 (2011).
92. M. G. Myers Jr., T. C. Grammer, L. M. Wang, X. J. Sun, J. H. Pierce, J. Blenis, M. F. White, Insulin receptor substrate-1 mediates phosphatidylinositol 3′-kinase and p70S6k signaling during insulin, insulin-like growth factor-1, and interleukin-4 stimulation. *J. Biol. Chem.* **269**, 28783–28789 (1994).
93. F. Peruzzi, M. Prisco, M. Dews, P. Salomoni, E. Grassilli, G. Romano, B. Calabretta, R. Baserga, Multiple signaling pathways of the insulin-like growth factor 1 receptor in protection from apoptosis. *Mol. Cell. Biol.* **19**, 7203–7215 (1999).
94. D. J. Van Horn, M. G. Myers Jr., J. M. Backer, Direct activation of the phosphatidylinositol 3′-kinase by the insulin receptor. *J. Biol. Chem.* **269**, 29–32 (1994).
95. B. Vanhaesebroeck, J. Guillermet-Guibert, M. Graupera, B. Bilanges, The emerging mechanisms of isoform-specific PI3K signalling. *Nat. Rev. Mol. Cell Biol.* **11**, 329–341 (2010).
96. M. Wiznerowicz, D. Trono, Conditional suppression of cellular genes: Lentivirus vector-mediated drug-inducible RNA interference. *J. Virol.* **77**, 8957–8961 (2003).

97. A. Funahashi, M. Morohashi, H. Kitano, N. Tanimura, CellDesigner: A process diagram editor for gene-regulatory and biochemical networks. *BIOSILICO* **1**, 159–162 (2003).
98. S. Hoops, S. Sahle, R. Gauges, C. Lee, J. Pahle, N. Simus, M. Singhal, L. Xu, P. Mendes, U. Kummer, COPASI—A COmplex PAthway SImulator. *Bioinformatics* **22**, 3067–3074 (2006).
99. A. Corana, M. Marchesi, C. Martini, S. Ridella, Minimizing multimodal functions of continuous variables with the "simulated annealing" algorithm. *ACM Trans. Math. Softw.* **13**, 262–280 (1987).
100. S. Kirkpatrick, C. D. Gelatt Jr., M. P. Vecchi, Optimization by simulated annealing. *Science* **220**, 671–680 (1983).
101. H. Schmidt, M. Jirstrand, Systems Biology Toolbox for MATLAB: A computational platform for research in systems biology. *Bioinformatics* **22**, 514–515 (2006).
102. S. M. Keating, B. J. Bornstein, A. Finney, M. Hucka, SBMLToolbox: An SBML toolbox for MATLAB users. *Bioinformatics* **22**, 1275–1277 (2006).
103. M. Hucka, A. Finney, H. M. Sauro, H. Bolouri, J. C. Doyle, H. Kitano, A. P. Arkin, B. J. Bornstein, D. Bray, A. Cornish-Bowden, A. A. Cuellar, S. Dronov, E. D. Gilles, M. Ginkel, V. Gor, I. I. Goryanin, W. J. Hedley, T. C. Hodgman, J. H. Hofmeyr, P. J. Hunter, N. S. Juty, J. L. Kasberger, A. Kremling, U. Kummer, N. Le Novere, L. M. Loew, D. Lucio, P. Mendes, E. Minch, E. D. Mjolsness, Y. Nakayama, M. R. Nelson, P. F. Nielsen, T. Sakurada, J. C. Schaff, B. E. Shapiro, T. S. Shimizu, H. D. Spence, J. Stelling, K. Takahashi, M. Tomita, J. Wagner, J. Wang; SBML Forum, The systems biology markup language (SBML): A medium for representation and exchange of biochemical network models. *Bioinformatics* **19**, 524–531 (2003).
104. R Development Core Team, *R: A Language and Environment for Statistical Computing* (R Foundation for Statistical Computing, Vienna, Austria, 2005), Version 2.12.1.
105. H. Akaike, A new look at the statistical model identification. *IEEE Trans. Automat. Contr. AC* **19**, 716–723 (1974).

Acknowledgments: We thank P. Polak, T. B. L. Kirkwood, G. Smith, and A. Merz-Biro for critical reading of the manuscript. We thank B. Holzwarth for technical assistance. We also thank our reviewers for critical and constructive input. **Funding:** This work was supported by the European Council 6th FP NoE LifeSpan (LSHG-CT-2007-036894 to D.P.S., K.T., and R.B.), the Schlieben-Lange-Programm (K.T.), the Excellence Initiative of the German Federal and State Governments (EXC 294 to K.T., R.B., and T.B.H.; FRIAS LifeNet to R.B.), Bundesministeriums für Bildung und Forschung GerontoSys II–NephAge (031 5896A) (K.T., T.B.H., and R.B.), and Deutsche Forschungsgemeinschaft grant P7-KFO 201 (T.B.H., R.B., and E.N.-H.). **Author contributions:** K.T., D.P.S., and R.B. planned and guided the project. K.T. and D.P.S. conceived and designed the experiments. P.D.P., A.G.S., S.F., A.T., and M.T.P. performed the experiments. K.T., D.P.S., P.D.P., and A.G.S. analyzed the data. A.T., T.B.H., M.G., and E.N.-H. contributed reagents, materials, and analysis tools. K.T. and D.P.S. wrote the paper. A.G.S. and P.D.P. contributed to manuscript writing. **Competing interests:** The authors declare that they have no competing interests. A part of this work is part of a pending European patent application, which has been filed on 1 June 2011 (application number 11004471.6-1225, Method for modelling, optimizing, parameterizing, testing and/or validating a dynamic network or network perturbation).

Submitted 26 August 2011
Accepted 8 March 2012
Final Publication 27 March 2012
10.1126/scisignal.2002469
Citation: P. Dalle Pezze, A. G. Sonntag, A. Thien, M. T. Prentzell, M. Gödel, S. Fischer, E. Neumann-Haefelin, T. B. Huber, R. Baumeister, D. P. Shanley, K. Thedieck, A dynamic network model of mTOR signaling reveals TSC-independent mTORC2 regulation. *Sci. Signal.* **5**, ra25 (2012).